3D geometry of the Dugald River Shear Zone, Mount Isa Inlier, Australia

P. K. Creus, I. V. Sanislav & P. H. G. M. Dirks

Published online: 28 Oct 2024.

Submit your article to this journal ↗

View related articles ↗

View Crossmark data ↗

Taylor & Francis
Taylor & Francis Group

3D geometry of the Dugald River Shear Zone, Mount Isa Inlier, Australia

P. K. Creus ⓘD, I. V. Sanislav ⓘD and P. H. G. M. Dirks ⓘD

Economic Geology Research Centre (EGRU) and Department of Earth and Environmental Sciences, James Cook University, Townsville, QLD, Australia

ABSTRACT

The Dugald River Shear Zone is a structurally complex, anastomosing shear zone that hosts high-grade Zn mineralisation within the Dugald River Slate. The Dugald River Zn–Pb–Ag mine is situated within the Mount Isa Inlier, Australia and developed through two phases of mineralisation with high-grade Zn mineralisation intimately associated with the development of the brittle–ductile Dugald River Shear Zone. The first phase of mineralisation occurred during the regionally extensive, D_2 ductile fold and axial planar cleavage forming event and resulted in the development of a sulfide horizon. This horizon was a preferential site for strain partitioning during early D_4 ductile deformation, which resulted in transposition-related concentration and thickening of a sulfide horizon marking the second phase of mineralisation. The Dugald River Shear Zone developed during D_4 wherein strain rate incompatibilities between a ductile-deforming sulfide horizon and the brittle-deforming Dugald River Slate resulted in the development of a Riedel shear zone. A high-resolution 3D model of the shear zone was constructed from robust drilling and mapping datasets in which releasing and restraining bends highlight the thickening and thinning of ore lenses, respectively. The 3D model with detailed structural analysis and observations allows for predictive modelling of dilational zones within throughgoing Y-shears, which are prospective sites for remobilisation of high-grade Zn sulfides as the ore body developed coevally with progressive shearing.

KEY POINTS
1. Detailed structural analysis provides 3D modelling parameters and exploration vectors.
2. The Dugald River Shear Zone developed as an evolved Riedel shear network during dextral transpression.
3. Understanding the shear zone's 3D geometry and kinematics allows for predictive modelling of ore lens distribution and identification of dilational zones, which are crucial for exploration and mining strategies.

Introduction

In the mining industry, 3D geological models of the subsurface form the foundations for optimised mining. Publications that use implicit 3D models as a basis for presenting complex structural and orebody geometries have recently gained traction, in part owing to workflow-based implicit modelling software, which allows researchers to quickly produce a model and discuss a wide range of topics such as ore-body geometries (*e.g.* Basson, McCall *et al.*, 2018; Basson, Thomas *et al.*, 2018; Hill *et al.*, 2014; Hillacre *et al.*, 2021; Kitt *et al.*, 2018; Stoch *et al.*, 2018; Vollgger *et al.*, 2015, 2020) and country-rock framework to intrusive bodies such as kimberlites and carbonatites (*e.g.* Basson *et al.*, 2016, 2017; Creus *et al.*, 2018).

In this contribution, we discuss the structural analysis, development and 3D modelling of the Dugald River Shear Zone and its role in hosting high-grade Zn–Pb mineralisation. Shear and fault zones have long been recognised as important channel ways for focusing and transporting fluids from depth (*e.g.*

Hobbs, 1987; Sibson, 1990) and for creating dilatancy in step-overs and releasing bends (*e.g.* Davis & Reynolds, 1996; Ford *et al.*, 2009; Hillacre *et al.*, 2021; Micklethwaite *et al.*, 2015). Dilatant zones assume a crucial function in the remobilisation and concentration of minerals, such as sulfides, as they are zones of volume increase owing to structurally induced increased porosity and permeability. Thus, identifying and delineating dilatant zones within a shear zone is paramount for optimised mining, as these volumes will represent localities of enhanced mineralisation associated with thicker ore lenses. Furthermore, their efficacy of hosting economic mineralisation is dependent on several factors including dip angle of the structure, lithological contrast, width of structure and geometry of the bend, as demonstrated using numerical modelling by Ford *et al.* (2009).

The Dugald River Shear Zone is structurally complex and, combined with the graphitic nature of the slate (Creus *et al.*, 2023; Newberry *et al.*, 1993; Xu, 1996), necessitates close drill spacing to delineate the shear zone and proximal ore body, in

turn to ensure safe and optimised underground mining (Harris, 2015). While planar structural data such as shear and foliation measurements can be incorporated in implicit modelling to construct complex geometries such as folds and faults (Cowan et al., 2003; Grose et al., 2021; Hillier et al., 2014; Laurent et al., 2016), drilling into structurally complex shear zones may not return drill core in which structures can be accurately measured. Thus, qualitative structural data are often the only data available within the rock mass in shear-zone hosted deposits. Furthermore, structural data such as faults and shears are generally not classified during mapping and logging, as clear distinguishing characteristics are often lacking, and, in an anastomosing shear zone, a single drill hole may intercept numerous shears, making classification difficult and time-consuming during logging. Thus, classification of discrete structures is performed explicitly during modelling. This study details a methodology for constructing a high-resolution, implicit 3D model of a complex, anastomosing mineralised shear zone.

Geological setting

The Dugald River Shear Zone, situated in the metallogenically significant Late Paleoproterozoic Mount Isa Inlier, hosts the Dugald River Zn–Pb–Ag deposit (Figure 1). The elevated Zn grade of the Dugald River Zn–Pb–Ag deposit is hosted within the graphitic Dugald River Slate of the Mount Albert Group, which was deposited during the 1730–1640 Ma Calvert Superbasin event (see Gibson et al., 2016). The geological history of the Mount Isa Inlier is complex and has been the focus of detailed research over decades, which describes the
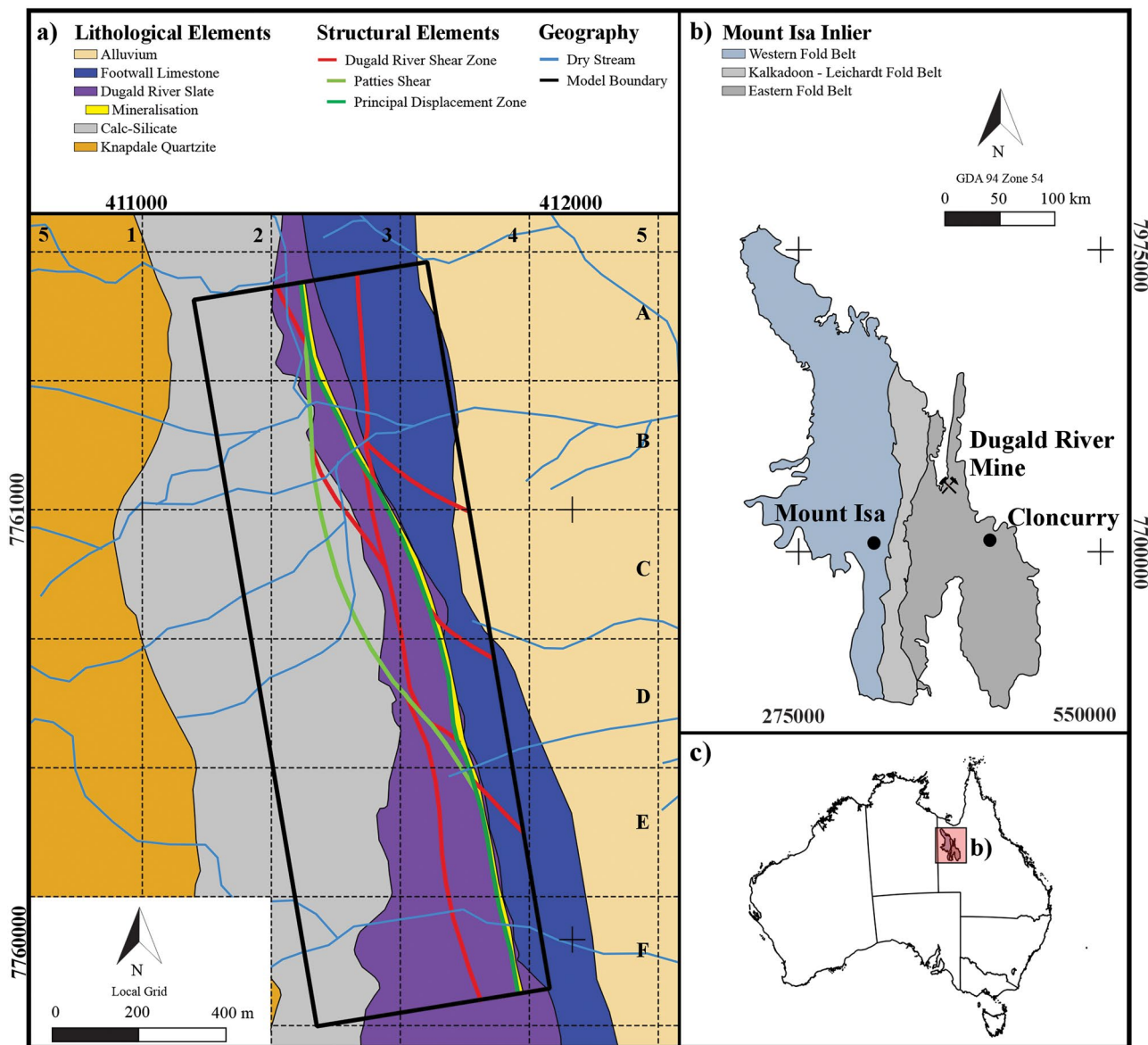
Figure 1. (a) Geological map of the Dugald River deposit. A local grid comprising the letters A–F and numbers 1–5 is used in this study to provide a spatial reference for figures. The Patties Shear Zone and the principal displacement zone are significant shears that form part of the Dugald River Shear Zone. (b) Outline of the Mount Isa Inlier using the traditional subdivision of threefold belts. (c) Location of the Mount Isa Inlier in northwest Queensland, Australia.

succession of volcano-sedimentary and igneous rocks formed during a series of successive basin and orogenic events during *ca* 1900–1500 Ma, and the reader is referred to key publications for more detail (*e.g.* Blake, 1987; Blake & Stewart, 1992; Foster & Austin, 2008; Gibson *et al.*, 2016; Jackson *et al.*, 2000; Le *et al.*, 2021a, 2021b; Rubenach *et al.*, 2008; Scott *et al.*, 2000; Spence *et al.*, 2021, 2022; Withnall & Hutton, 2013). In this section, we provide a summary of the Mount Isa Inlier relevant to the development of the Dugald River Shear Zone and followed by a description of the local geology.

Mount Isa Inlier

The framework of the Mount Isa Inlier comprises 16 tectonic domains with a general north–south trend, grouped for simplicity into the Western and Eastern fold belts that are separated by the Kalkadoon–Leichhardt Belt (Figure 1b). The domains are superimposed on major depositional basins and basement that were deposited during three main depositional events (*e.g.* Gibson *et al.*, 2016): the Leichhardt Superbasin (1790–1740 Ma), Calvert Superbasin (1730–1640 Ma) and the Isa Superbasin (1640–1590 Ma). Three orogenic events have affected the Mount Isa Inlier (see Blake, 1987; Blake & Stewart, 1992; Foster & Austin, 2008; Spence *et al.*, 2021, 2022): the 1880–1850 Ma Barramundi Orogeny, the 1750–1710 Ma Wonga Orogeny and the 1650–1490 Ma Isan Orogeny.

The final, major orogenic event is generally accepted as the 1650–1490 Isan Orogeny (Blake 1987; Blake & Stewart 1992; Foster & Austin 2008). The Isan Orogeny is associated with up to five regional deformation events. An initial phase of north–south-directed shortening (D_1) produced east–west-trending regional folds and thrusts (*e.g.* Abu Sharib & Sanislav, 2013; Bell, 1983, 1991; Lister *et al.*, 1999; Page & Bell, 1986; Withnall & Hutton, 2013). The second event (D_2) is regarded as the main deformational event that produced the north–south-trending structural grain of the Mount Isa Inlier (*e.g.* Abu Sharib & Bell, 2011; Abu Sharib & Sanislav, 2013; Bell *et al.*, 1992; Foster & Rubenach, 2006; Giles *et al.*, 2006; Withnall & Hutton, 2013). D_2 structures formed owing to east–west shortening that produced regional north–south-trending folds, shears and thrusts, together with a pervasively developed S_2 foliation and peak metamorphism (M_2) that reached upper amphibolite facies. The third deformational event (D_3) is associated with an inferred period of orogenic collapse that produced a subtle, subhorizontal fabric, which includes low-angle thrusts, F_3 folds that locally rotate earlier fabric elements and a spaced S_3 cleavage (*e.g.* Bell & Hickey, 1998; Creus *et al.*, 2023; Davidson *et al.*, 2002; Murphy, 2004; Xu, 1996). A fourth deformational event (D_4) marks the transition from ductile to brittle–ductile deformation during renewed east–west-directed shortening and had a pronounced transpressional character (*e.g.* Bell & Hickey, 1998; Creus *et al.*, 2023; O'Dea *et al.*, 1997; Spampinato *et al.*, 2015). This event is defined by the development of high-strain fabrics (S_4) and anastomosing shear zones. The final major deformation event (D_5) resulted from east-northeast–west-southwest shortening and involved brittle reactivation of major structures (*e.g.* Creus *et al.*, 2023; Xu, 1996).

Mount Roseby Corridor

The Mount Albert Group comprises mixed carbonate–siliciclastic rocks that were deposited towards the end of the Calvert Superbasin infill, which are subdivided into four main units, *viz.* the Knapdale Quartzite, the Lady Clayre Dolomite, the Coocerina Formation and the Mount Roseby Schist (Figure 1a; Foster & Austin, 2008; Withnall & Hutton, 2013). Age dating by Carson *et al.* (2009, 2011) provided maximum depositional ages for the Lady Clayre Dolomite and Mount Roseby Schist of 1691 Ma and 1686 Ma, respectively. The Mount Albert Group underlies a complexly deformed high-strain corridor referred to as the Mount Roseby Corridor (see Creus *et al.*, 2023; Newberry *et al.*, 1993), characterised by generally steep, west-dipping strata with local variations to the east-related to east-verging folding. The Mount Roseby Corridor is bounded by strike-extensive faults with the Mount Roseby Fault defining the eastern boundary and the Coolullah Fault, the western boundary. The Mount Roseby Schist constitutes the eastern half of the Mount Roseby Corridor and comprises a thick package of limestone, calc-silicate and the Dugald River Slates, which hosts the deposit (Figure 1a).

In the Mount Roseby Corridor, five deformational (D_1 to D_5) events associated with the Isan Orogeny have been recognised with successive deformation events progressing from ductile (D_1 to D_3) to brittle–ductile (D_4) and lastly brittle (D_5; Creus *et al.*, 2023; Newberry *et al.*, 1993; Xu, 1996). The first deformation event, D_1, is associated with north–south shortening in the Mount Isa Inlier (*e.g.* Abu Sharib & Sanislav, 2013; Bell, 1983, 1991; Page & Bell, 1986). At Dugald River Mine, structural elements associated with D_1 include east–west-trending folds (F_1) and an axial planar cleavage (S_1) preserved in outcrop 10 km to the south of the deposit (see Xu, 1996) and as inclusion trials within syn-D_2 porphyroblasts (Creus *et al.*, 2023). However, within the deposit, D_1 structural elements have largely been overprinted by subsequent deformation events.

The second deformation event, D_2, represents the dominant fabric observed within the Mount Isa Inlier (*e.g.* Abu Sharib & Bell, 2011; Abu Sharib & Sanislav, 2013; Bell *et al.*, 1992; Betts *et al.*, 2006) and the Mount Roseby Corridor (Creus *et al.*, 2023; Newberry *et al.*, 1993; Xu, 1996). Structural elements associated with D_2 consist of multi-scale, closed to isoclinal, north–south-trending folds (F_2) and a well-developed axial planar cleavage (S_2) developed during east–west-ductile shortening. F_1 was overprinted by F_2 and developed a Type 1 interference pattern (*e.g.* Creus *et al.*, 2023; Xu, 1996), which was disrupted during D_4 (Creus *et al.*, 2023). D_2 is responsible for the overall steep, west-dipping stratigraphy observed in the Mount Roseby Corridor and resulted from macro-scale, overturned and isoclinal folding with east-directed vergence. A penetrative, north–south-trending S_2 foliation developed in all units and exhibits a steep westerly dip, with localised easterly dips. An initial phase of subeconomic mineralisation occurred towards the end of D_2 (Phase 1 mineralisation; Creus *et al.*, 2023) and is associated with progressive fold tightening during which flexural slip, hinge-normal and layer-normal quartz–carbonate veins were progressively rotated into parallelism with the pervasively developed S_2 fabric, and coevally replaced by sulfides. During fold tightening, hinge separation and boudinage along the fold limbs occurred.

A period of orogenic collapse, D_3, resulted in heterogeneously developed, low-strain deformation and associated subtle structures (*e.g.* Bell & Hickey, 1998; Creus *et al.*, 2023; Davidson *et al.*, 2002; Murphy, 2004; Xu, 1996). In the Mount Roseby Corridor, a weak S_3 cleavage developed within the Dugald River Slate, where it is associated with millimetre-scale crenulations and a disjunctive cleavage developed in the Footwall Limestone (Creus *et al.*, 2023). The S_3 cleavage has consistent southwest dips and Xu (1996) described subhorizontal folds (F_3) on surface and Davis (2017) in underground development. Zones of S_3 intensification are heterogeneously developed within the southern part of the Dugald River Mine with localised rotation of S_0 and S_2 into moderate southwest dips (Creus *et al.*, 2023; Xu, 1996). D_3 is associated with a subvertical principal stress direction (Creus *et al.*, 2023) and a top-to-the-east sense of shear (Davis, 2017; Xu, 1996). Notably, zones of intense S_3 were reactivated during early D_4 as low-angle thrusts with a top-to-the-northeast sense of shear (Creus *et al.*, 2023), and these segmented the Phase 1 mineralisation and major stratigraphic horizons.

In a complementary study to this contribution, Creus *et al.* (2023) suggested that brittle–ductile deformation during D_4 is responsible for the development of the Dugald River Shear Zone. In this study, we provide a detailed analysis of the progressive deformation during a D_4 event that resulted in development of the anastomosing shear zone that hosts the Zn–Pb mineralisation. Lastly, the final deformation event that may be recognised, D_5, is marked by reactivation of earlier fabrics (*e.g.* Creus *et al.*, 2023; Xu, 1996). The most striking result is the development of fault rocks (breccia and cataclasite), with cohesive and non-cohesive varieties that indicate active deformation at upper crustal levels.

Methods

The datasets used to construct the 3D geometry of the Dugald River Shear Zone include dense drilling data, underground mapping and photogrammetry-derived 3D reconstructions of development drives. In this section, we detail the structural datasets that were incorporated into the 3D model and highlight inadequacies with data or dataset types, which should be considered when constructing surfaces.

Drilling data

Prior to the commencement of mining activities in 2012, there were 467 pre-collared diamond core drill holes used to delineate the ore body. In subsequent years, an additional 2546 diamond drill holes were completed, mostly from underground development from 2015 to late 2019 (the data cutoff for the 3D model presented here). This significant increase in drilling followed a period of care and maintenance, during which the structural complexities at Dugald River Mine were resolved, after which a decision was made to reduce the drill-hole spacing (see Harris, 2015).

Drill programmes at the mine use a fan pattern with primary drill holes followed by infill drill holes. Primary drill holes, which are orientated have a spacing of 40 m along strike and 30 m down dip. Primary drilling is followed by non-orientated infill drilling at 15 m intervals along strike and 10 m intervals down dip in places where the structural geology is deemed complex (Figures 2 and 3; Harris, 2015). Although primary drill holes are orientated, the graphitic nature of the shear zone and degradation of discrete shears can prevent accurate orientated data capture. For a structure to be recorded as acceptable, orientation marks need to be linked over at least three successive drill-core runs. Thus, Spelbrink and George (2017) developed a method at Dugald River Mine to record structural data as intervals, with a structure (fault, breccia, shear, fracture) assigned a damage intensity rating increasing from 1 to 5 (Figure 3). In this manner, structural data can be imported as a categorised interval table and used within applicable modelling software. It should be noted that adjacent drill holes with logged intervals of, for example, fault intensity rating 5 do not necessarily intersect the same structure, considering that discrete structures in the shear zone can pinch and swell completely at a metre scale (Figure 3). An advantage of logging structures as intervals allows for modelling of the shear system as a closed surface that incorporates the damage zones of individual or discrete structures.

Mapping data

Face mapping by Mine Geologists was initially conducted as development progressed; however, this was phased out in 2017 and replaced by digital mapping using photogrammetry (SfM-MVS). SfM-MVS is a technology gaining popularity in underground mining (see Creus *et al.*, 2021 and references therein), as it allows for virtual outcrops to be recorded as 3D reconstructions (*e.g.* Figures 3 and 4) and measurements to be digitised using 3D modelling software. Geoscientists are limited to active mining areas, while safe mining practices limit accessibility only to safe, supported development faces. Thus, in a deposit like Dugald River where the ore body is adjacent to a moderate to subvertical shear zone, the geological features to be mapped are typically on development faces (*e.g.* Figure 4) that cannot be directly measured owing to safety concerns. At the time of the data cutoff for this study (end of 2019), a total of 5620 virtual outcrops were available, along with 4227 fault, shear and fracture points from face mapping by Mine Geologists prior to digitisation of virtual outcrops.

As part of the study, and to gain first-hand observations of the Dugald River Shear Zone, underground face mapping was conducted at the start of the study in early 2019. At that time, the mine was 7 years into active mining and at the 540 level (*viz*. 540 m below surface) with a ~2 km strike length exposed. Accordingly, a significant 3D volume of the deposit could be mapped, although, to limit mapping time, the South Mine was prioritised over the North Mine. The geometry of the shear zone and adjacent ore body is flatter in the South Mine and thicker, with multiple ore lenses (Creus *et al.*, 2023), multiple ore drives and linking cross-cutting drives, providing a
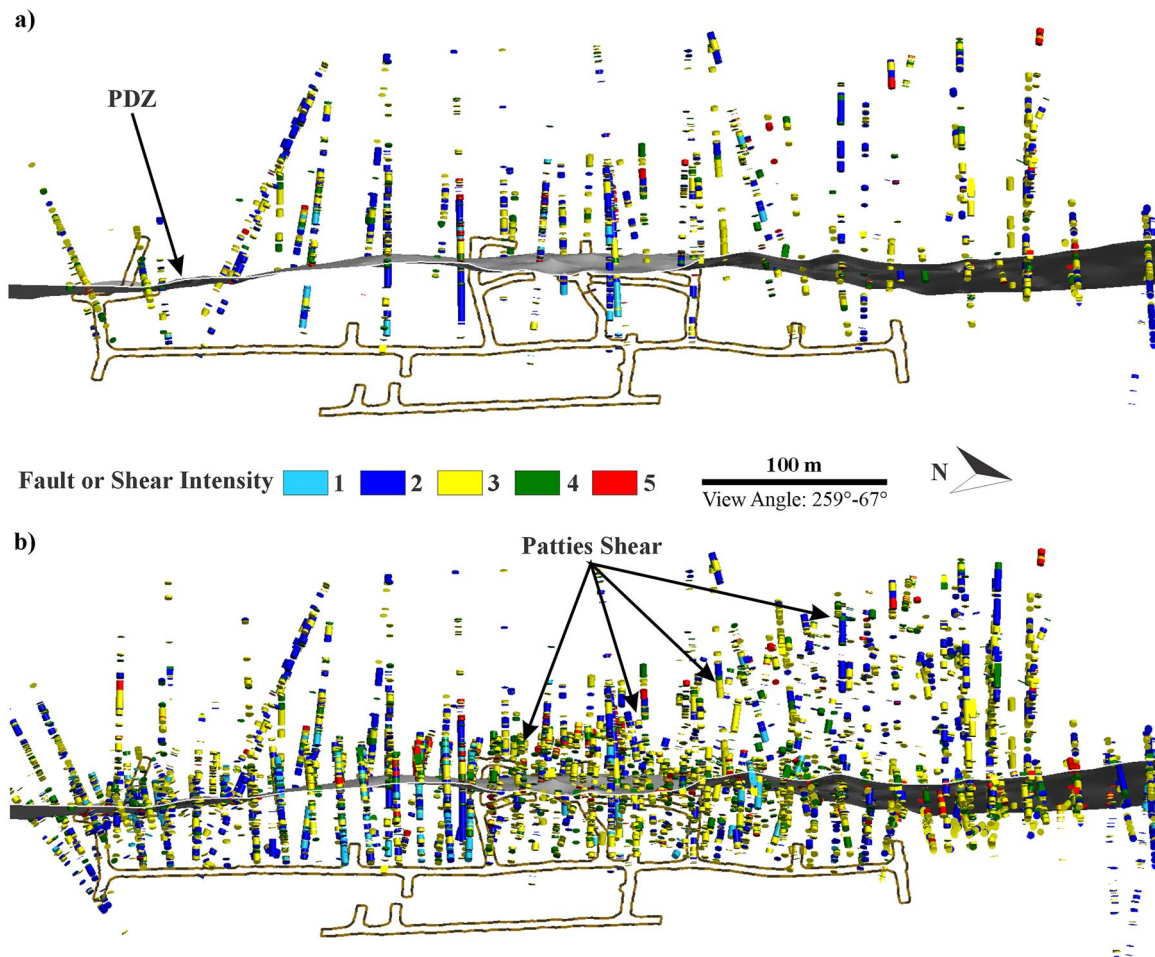
Figure 2. Comparison between (a) primary drilling at 40 m along strike and 30 m down-dip, and (b) including infill drilling at 15 m along strike and 10 m down-dip, as this is a structurally complex area (South Mine). The figure illustrates why there was a need to reduce the drill spacing, as shears are easier to visualise and assign drilling intervals to discrete shears. The development level shown here is S365 (*i.e.* 365 m below the surface).

comprehensive 3D overview of the deposit over several levels. In contrast, the shear zone and ore body in the North Mine are steeper and generally intersected by a single drive per level. It should be noted that the ore body at Dugald River Mine is accessed via two declines, in the limestone to the east (see Figure 5). Access drives are developed off declines towards the west, and in the North Mine, a single, north–south ore drive occurs along the footwall of the ore body, while in the South Mine—and at depth where the shear zone flattens—a north–south footwall drive is developed. Several west-striking cross-cuts are developed off the footwall drive and may have several north–south ore drives, depending on the thickness and geometry of the ore body.

Underground mapping conducted during this study was augmented by SfM-MVS 3D reconstructions. In areas that were deemed structurally complex, virtual outcrops were reprocessed (total of 2118) at a higher quality so that finer detail could be mapped. The virtual outcrops were imported into Leapfrog Geo (Seequent, 2021), and shear and fault planes were digitised as polylines in Leapfrog Geo, as the software allows for the polarity of the polylines to be set, which is necessary when modelling undulating, steep structures.

While digitising virtual outcrops for mapping purposes allows for augmenting of traditional mapping using a compass and clinometer, they should be stored in a separate table or a column provided in the mapping table, which specifies the source. With virtual outcrops, only the orientation, scale and type of structure can be recorded with confidence and limitations in what material properties may be recorded (*e.g.* lithology and alteration). Furthermore, virtual outcrops suffer from occlusion, or partial occlusion (see Cawood *et al.*, 2017), which may produce erroneous results along the sidewalls of development drives, so limiting mapping to faces of virtual outcrops is recommended. In contrast, traditional mapping allows for descriptive data collection, which includes coordinates, orientation, structure type, kinematic information, comments, material properties and classification of what is recorded, and importantly small-scale features such as striations, crenulations and porphyroblasts.

Consequently, mapping data were divided into characterised and orientation-only datasets (also Creus, 2022). Characterised mapping data refer to descriptive data, which include the coordinates, orientation, structure type, kinematic information, comments, material properties and classification
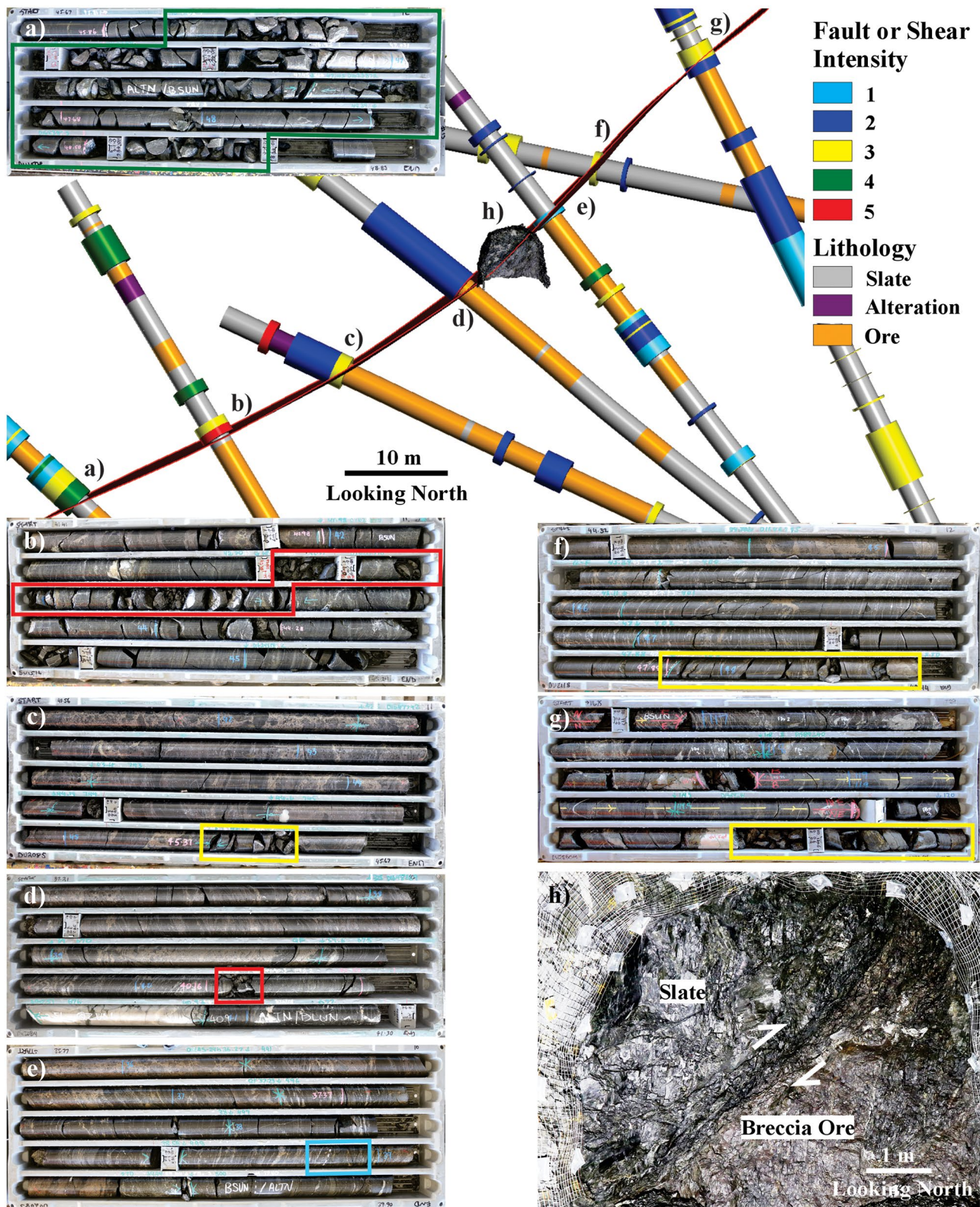
Figure 3. Example of logged intervals for shears and faults (grid reference: 4D). The structures are categorised as shears, faults or fault breccia, and assigned an intensity rating from 1 to 5. Shown in this figure is the footwall plane of the principal displacement zone, which, over a down-dip distance of several tens of metres, has a highly variable thicknesses that makes modelling difficult without orientation data. Thickness variation is partly due to reactivation of the structures during D_5 with metre-scale displacements observed [*e.g.* (h)].

of a feature. Accordingly, the characterised dataset represents high-confidence data that can be confidently used in interpretations and to determine modelling parameters. Orientated

mapping data generally only include coordinates, orientation and structure type; thus, they represent lower confidence data that may potentially introduce uncertainty or ambiguity into a
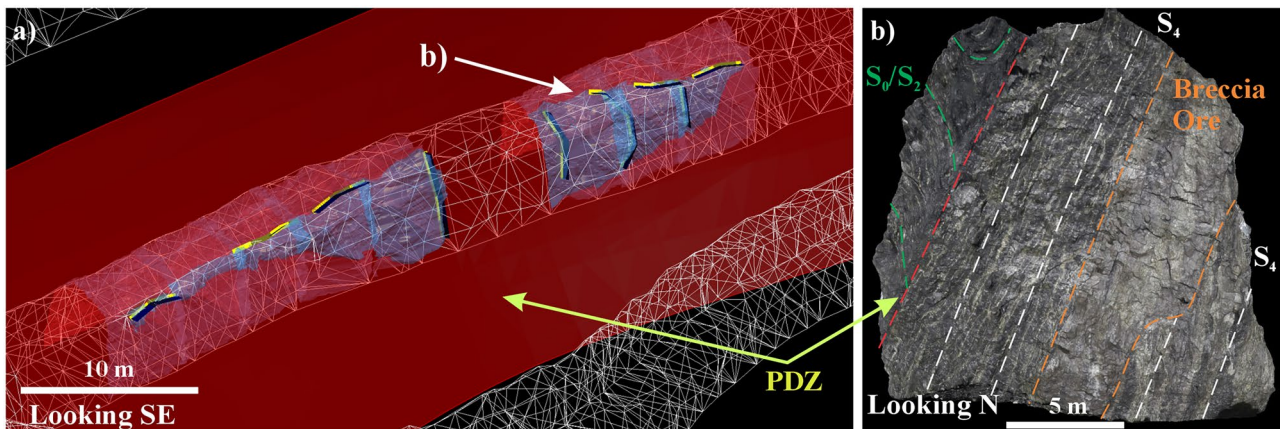
Figure 4. (a) Example of digitised polylines and associated modelled shears on the S220 level (220 m below surface; grid reference: 3C). Successive captures using SfM-MVS allow for polylines to be digitised directly on the face of the drives and incorporated into modelled shears. (b) In addition, ore lenses can be digitised and modelled as closed volumes, with polylines set with inside/outside tangents. PDZ, principal displacement zone.
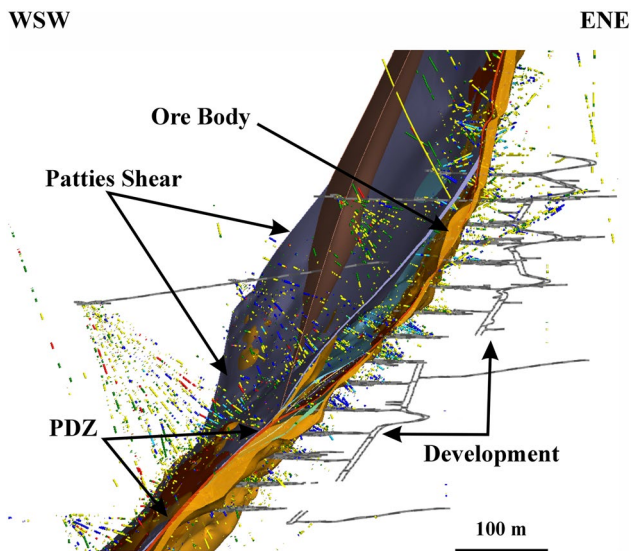
Figure 5. Cross-section through the South Mine. The shears are randomly coloured and generated as closed surfaces. Included are logged intervals for drilling data (see Figure 2 for colour codes of the intervals), illustrating the decreased drilling data away from the ore body, particularly towards the west (*viz.* hanging wall). Mapping data are biased towards the east of the shear zone, owing to the development in the footwall of the shear zone/ore body. PDZ, principal displacement zone (location of the cross-section shown in Figure 6).

model. Lastly, as most of the drives are north–south-trending, and to avoid bias to north–south-striking structures, east–west cross-cuts were prioritised during face mapping as part of this study.

3D geological model construction

The Dugald River Shear Zone is a complicated structure to model. In part, owing to the numerous shears and faults that comprise the anastomosing shear system, but mainly owing to its graphitic and reactivated character. Metre-wide ore lenses in the deposit tend to occur along the footwall of discrete shears, with the main ore lens positioned along the footwall of the principal displacement zone (*e.g.* Figure 3; Creus *et al.*, 2023). The principal displacement zone is also typically furthest

eastward and a significant discrete shear, with most shears modelled to its west (Figure 5). Thus, long-term mine development generally occurs to the east of the principal displacement zone, resulting in mapping data distribution that is biased towards the footwall and therefore adjacent to the shear zone. Undifferentiated mapping data for faults, shears and fractures are associated with the footwall total 18,772 for (a) face mapping obtained during this study and (b) face mapping by mine geologists and orientated vertices extracted from polylines. For the hanging wall, this total is 8433. West-trending cross-cuts required to exploit ore lenses to the west provide valuable information regarding the geometry and spacing of discrete shears, as they intersect the sidewall of drives and can be observed directly using standard mapping.

In this study, we used Leapfrog Geo (Seequent, 2021) and SKUA-GOCAD (Paradigm, 2021) with the GOCAD Mining Suite extension (Mira Geoscience, 2021) for interpreting structural data and modelling the Dugald River Shear Zone. Only discrete shears that could be linked across multiple levels and drives were modelled. A wireframe surface resolution of 4 m in the mine coordinate system was set, which is approximately the development cut spacing. Two models for the Dugald River Shear Zone were constructed: (1) footwall planes of discrete shears (Active Model, *e.g.* Figure 6) and (2) closed surface model (*e.g.* Figure 5).

Active model

The active model was built using wireframe surfaces that represent the footwall planes of discrete shears. Footwall planes were used because observations in drill core and underground development indicate that sulfide mineralisation is concentrated along the footwall of discrete shears. Furthermore, by modelling individual wireframe surfaces, structural domains can be defined, to allow for discretised modelling of ore lenses and the generation of form surfaces that broadly represent the main plane of anisotropy (*e.g.* Creus *et al.*, 2019).

Discrete shears were identified using mapping data, which as a minimum have orientation information associated with them, although higher confidence data were given priority. For

South Mine　　　　　　　　　　　　　　　　　　　**North Mine**
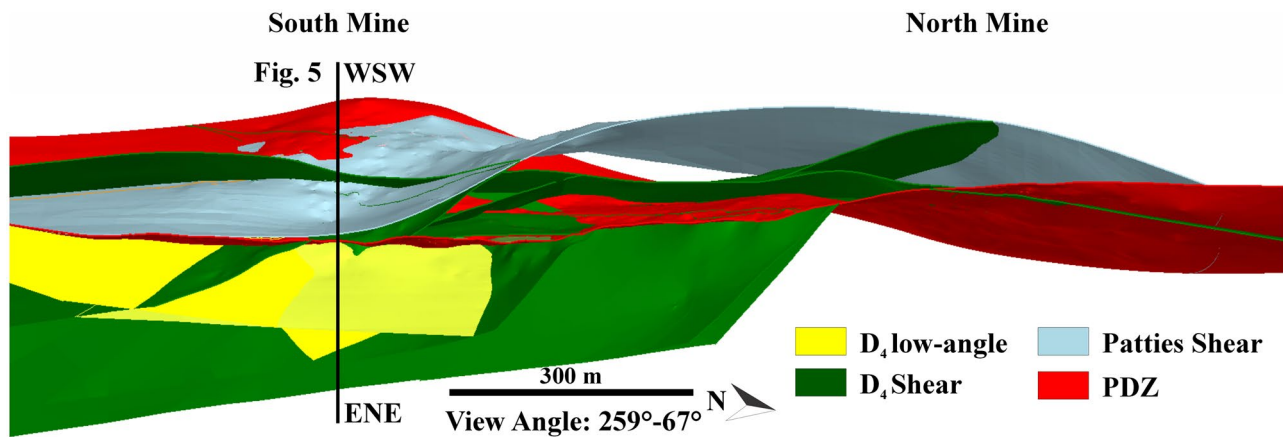
Figure 6. Down-dip view of the Dugald River Shear Zone within the model boundary. The mine is subdivided into a North and South Mine with each mine accessed by a decline and linked occasionally by throughgoing development drives. Zones of intensified S_3 were reactivated during D_4 as arrays of low-angle thrusts (yellow planes, Creus *et al.*, 2023) and are pronounced in the South Mine (grid reference: 4D). The location of the cross-section (Figure 5) is shown.

instance, multiple data points within proximity to one another commonly have variable orientation, and owing to the higher confidence rating of characterised data, these should be preferentially included in wireframe construction. In the construction of the Dugald River Shear Zone, mapping data that could be linked across multiple levels and drives were assigned to the same shear (Figure 7). The principal displacement zone is the primary surface with all other relevant surfaces terminating against it. A second prominent shear, the Patties Shear, developed towards the west of the principal displacement zone (*e.g.* Figures 1 and 6).

Intervals from drilling data were added to the shears by using the 'Vein' tool in Leapfrog Geo. The vein tool generates a hanging wall and footwall wireframe surface from either the start or end-points of a drill-hole interval, depending on the orientation of the connection points. The necessary points were added to the wireframe surfaces. This process requires iterations of selecting and adding data to the wireframe surfaces to extend them into the rock mass, and as the Dugald River Shear Zone is anastomosing, the extended wireframe surfaces may overlap closely with one another. In these instances, the wireframe surfaces are merged to create a single wireframe surface (Figure 7).

Closed surface model

The closed surface model (*e.g.* Figure 5) was generated in the same manner as the Active Model, with hanging wall data included. Using the same shear hierarchy as the active model, a continuous shear zone was modelled that represents the discrete shears of the Dugald River Shear Zone. With the closed surface model, the damage zones of the shears and faults can be represented in 3D and aid mine design.

### Structural analysis of D_4 elements

Multiple deformational events during the Isan Orogeny have been recognised in the Mount Isa Inlier and the Mount Roseby Corridor. The consensus is that the dominant deformational events are: (1) D_2, which imparted the regional north–south

structural grain of the Mount Isa Inlier (*e.g.* Bell *et al.*, 1992, Withnall & Hutton, 2013); and (2) D_4 with its pronounced transpressional character that marked the transition from ductile to brittle–ductile deformation (*e.g.* Bell & Hickey, 1998; O'Dea *et al.*, 1997). The D_2 and D_4 events are both regarded as subhorizontal and east–west-directed, producing a subvertical fabric. Differentiating fabrics between those formed during D_2 and D_4 can be difficult even in underground mines with well-exposed outcrop. In this section, the results of a detailed structural analysis are presented with an emphasis on (1) the high-strain fabric development that overprinted earlier ductile fabric, and (2) the subsequent development of shears and faults that define the Dugald River Shear Zone.

Transposition and high-strain fabric

Within the Dugald River Mine, the D_2-related fabric is characterised by close to isoclinal F_2 folds and an associated axial planar cleavage, S_2. Creus *et al.* (2023) suggested that an early phase of mineralisation (Phase 1 mineralisation) is associated with progressive fold tightening whereby secondary fold accommodation structures such as veins progressively intensified and rotated parallel to subvertical fold axial planes (also Davis, 2017) while coevally being replaced by sulfides. In D_2 high-strain domains, alternating veins and slate layers are the easiest to recognise in terms of overprinting relationships with the D_4 fabric, particularly in the North Mine where a transposition fabric has developed, and metre-scale low-strain domains of folded D_2 fabric are wrapped by S_4 (Figure 8).

In the northern part of the mine, high-strain zones are marked by a transposed fabric that forms S_4 domains, from centimetre to metre scale, that wrap around low-strain domains that preserve older fabric elements (Figure 8; also Xu, 1996). In zones of transposed fabric, S_0, S_2 and Phase 1 mineralisation were rotated to form metre-scale zones of concentrated planar ore, referred to as early Phase 2 mineralisation, forming a pseudostratigraphy (Creus *et al.*, 2023). Macro-scale examples of transposition are visible on the surface to the north of the mine (Figure 8a).
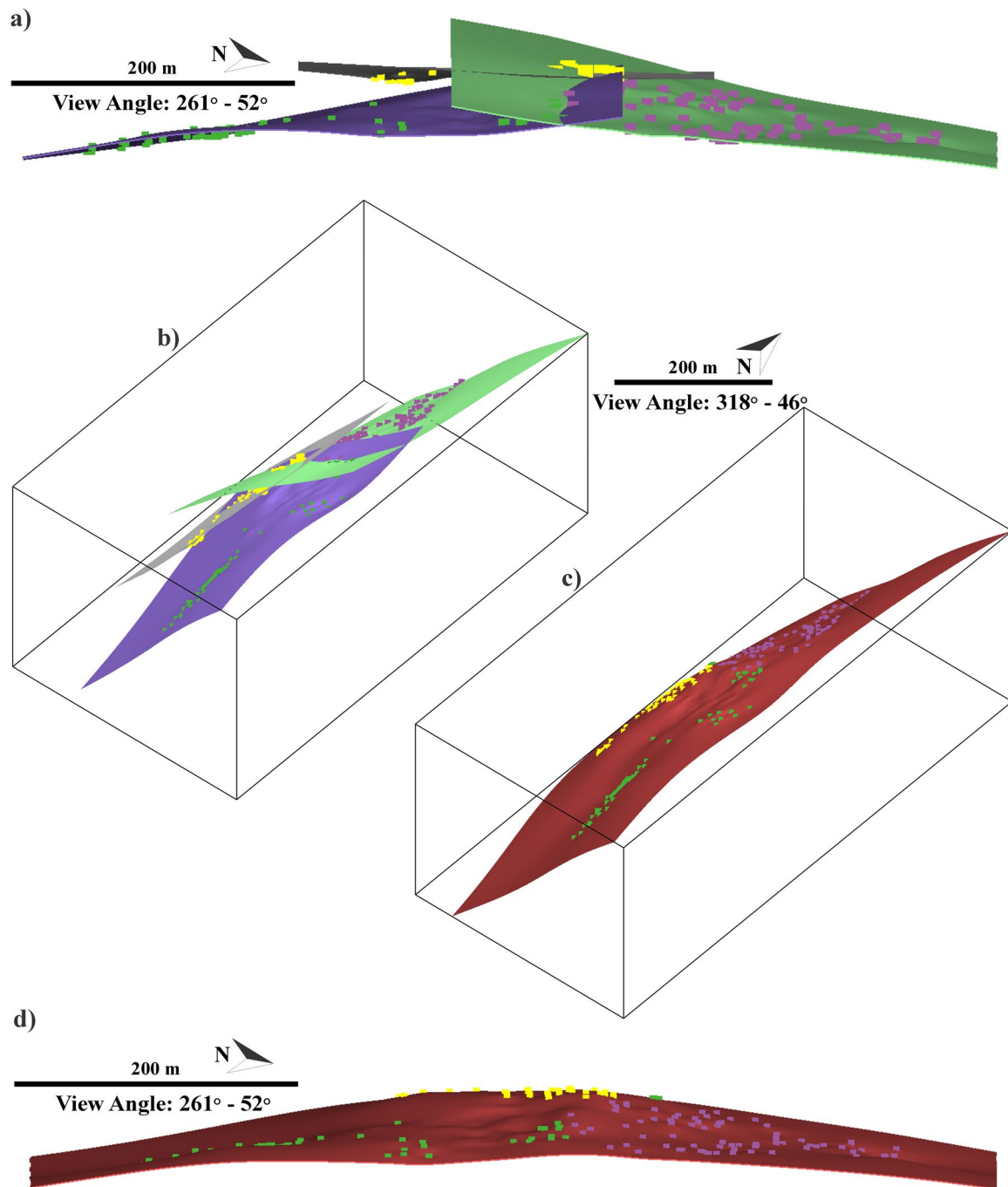
Figure 7. Modelling methodology to illustrate how footwall planes of the Active Model were modelled. (a) Mapping, including traditional techniques and SfM-MVS, was used to build initial surfaces, which were then used to guide what intervals from drilling should be assigned to the surface. (b) Oblique view of (a). (c) Oblique view of shears that were deemed to be part of a discrete shear. (d) Down-dip view of (c).

Mesoscale, shear-related, lozenge-shaped domains are common in the northern part of the mine (Figure 9). Lozenges represent low-strain domains that are enveloped by high-strain shear bands that curve into the D_4 fabric. Within low-strain domains, rotation of the pseudostratigraphy has occurred. Notably, shear bands are regarded by Williams and Price (1990) as indications of transpression when the main plane of anisotropy (here steep, west-dipping S_2) is subparallel to the shear margin (also see Ponce et al., 2013). Oblique shearing during transpression results in a sigmoidal geometry for lozenges and

synthetic slip with respect to the bulk shear direction along shear bands and has resulted in antithetic rotation of earlier D_2 related fabric.

The S-C′ fabric lenses are marked by penetrative, sigmoidal S-foliation displaced C′-planes. The overall asymmetry of lenses indicates a top-to-the-northeast sense of shear. Localised reversal of shears indicates that top-to-the-west shear along steep, east-dipping segments of shears has occurred (Figure 10a). The main S-foliation is penetrative and, in part, defined by the preferred orientation of graphite. Sigmoidal lenses in the S-C′ fabric
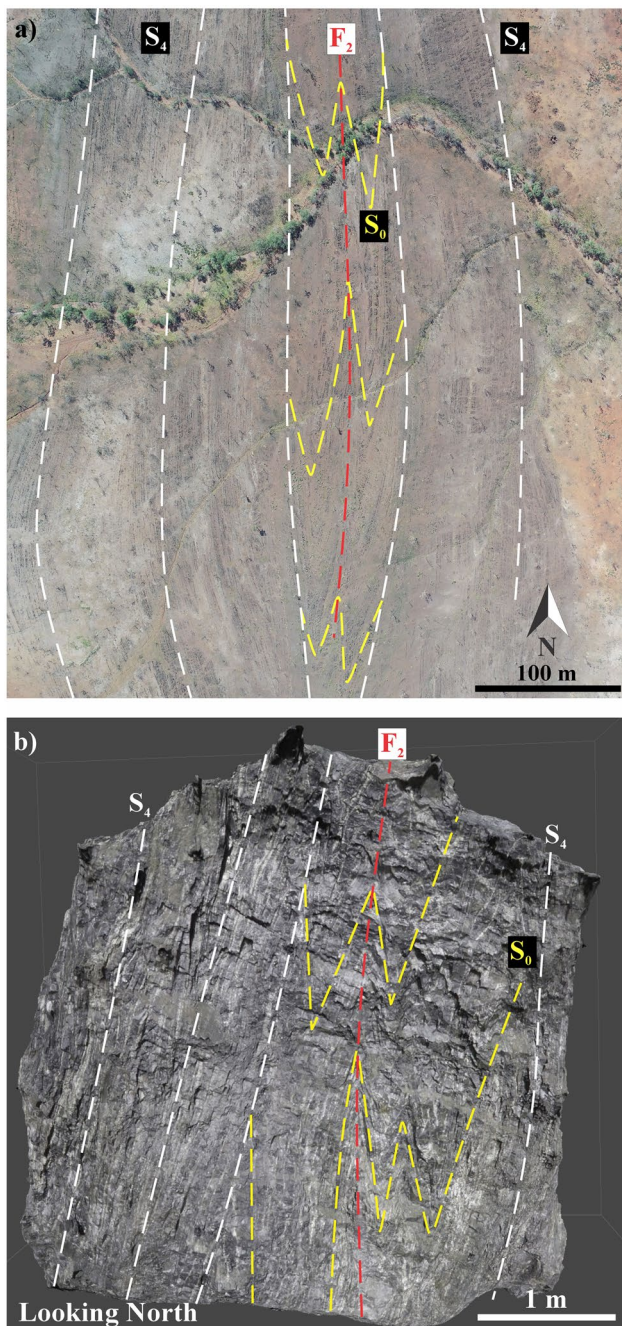
Figure 8. D_4-related transposition of earlier fabric (S_0, F_2, S_2 and Phase 1 mineralisation). (a) Drone image captured to the north of the deposit (coordinates GDA94 z54: 411520; 776227). Intense progressive deformation resulted in the transposition of S_0 and F_2 into high-strain domains representing S_4 that wrap around a lower-strain domain with preserved S_0 and F_2. (b) Structure-from-Motion Multiview Stereo (SfM-MVS) capture of N150_OD486_S level (grid reference: 3B). Here S_4 comprises transposed S_0, S_2, F_2 and Phase 1 mineralisation, and represents a high-strain domain that wraps around a lower-strain domain with preserved S_0 and F_2 folds and D_2-related secondary accommodation mechanism veins. The veins contain sulfide-replaced quartz–carbonate infill.

Figure 9. Simple shear-related lozenge common in the North Mine. Image of a development face captured on the N220_OD491_N level (grid reference: 3A). The asymmetry of the lozenges suggests a top-to-the-northeast sense of shear, thus east-northeast–west-southwest shortening during D_4.

of high- and low-strain domains and sporadic distribution of S-C′ fabric zones within high-strain zones are indicative of strain partitioning.

Shears and faults

The most striking feature in the Dugald River Mine is the Dugald River Shear Zone. From a qualitative perspective, the shears and faults within the shear envelope of the Dugald River Shear Zone lack distinctive characteristics to differentiate discrete features that can be linked between levels and drives. In general, wider shears have a variation in internal textures, from well-developed ductile shear fabrics, which can have a high graphite content, to incohesive cataclasite and fault breccia, which, according to Creus *et al.* (2023), is due to reactivation during D_5. Asymmetrical internal fabric (*e.g.* S-C′ fabric) within shears indicates hanging wall up movement, and cataclastic zones are inferred to be reactivated zones of the S-C′ fabric (also Creus *et al.*, 2023).

In this study, a semi-quantitative approach was used to differentiate discrete structures. Plotting the mapping data collected during underground face mapping during this study on a stereonet yielded inconclusive results, other than that there are two broad populations, with poles to planes centred at 260°/65° and 117°/77° (Figure 11). Furthermore, the Dugald River Shear Zone developed within the Dugald River Slate, and

have a fractal characteristic, and when picked up, lenses crumble into smaller lenses along the S-foliation and C′-planes (Figure 10c). The core of lenses is composed of sulfides, including sphalerite, which we suggest indicates that the S-C′ fabric developed after the transposed fabric developed. The presence
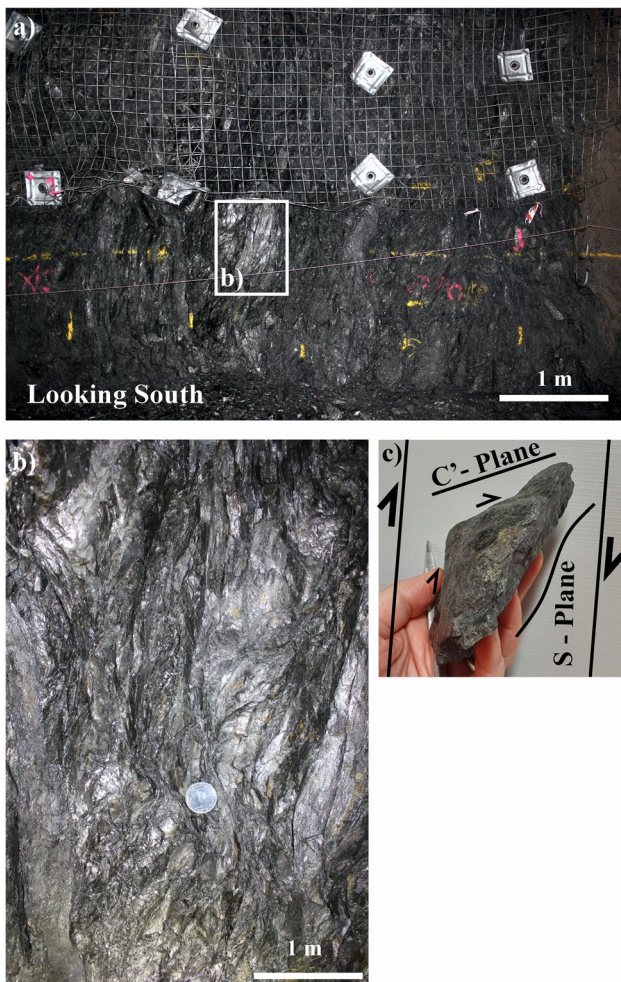
Figure 10. S-C′ fabric developed within a D₄-related high-strain zone. (a, b) Principal displacement zone on the S390_XC395_W level with a localised steep, easterly dip (grid reference: 4E). The image is taken from a cross-cut and, given the vertical dip of the shear zone, indicates the potential width of discrete shears within the shear zone. The width of the shear zone is ~20 m and extends to the west (covered by shotcrete). (c) Example of a sigmoidal lens created by the interaction of S-foliation and C′-planes.

so marker horizons are lacking, and striations on shear and fault planes were found to be inconclusive, owing to the graphitic nature of the shear zone. To separate the structural data into sets, the method outlined in *Active model* was used to model wireframes, from structural data, that could be confidently linked to a discrete structure. Geometrically, five orientations were observed, four of which, when plotting the face-mapping data from this study on stereonets, indicate the distinctive pattern of a Riedel shear network (Figure 12a).

Riedel shear network

A detailed structural analysis was undertaken on D₄-related structural elements, from which we concluded that the Dugald River Shear Zone developed as a transpressional, dextral, Riedel-like shear network (Figures 6 and 12). We use the term Riedel-like shear network, as the Dugald River Shear Zone does not fit the *sensu stricto* definition of a Riedel shear network, which was

initially defined using analogue experiments on clay (Riedel, 1929), repeated numerous times over the decades using either clay or sand (*e.g.* Barcos *et al.*, 2016; Naylor *et al.*, 1986; Tchalenko, 1968) and, with the aid of computers, numerical experiments (*e.g.* Chemenda *et al.*, 2015; Cho *et al.*, 2008; McKinnon & de la Barra, 1998).

The classic interpretation of Riedel shear zone geometries is that in the early stages of strike-slip fault formation, displacement within basement rocks produces characteristic fault geometries within the overlying cover (*e.g.* Arboleya & Engelder, 1995; Tchalenko, 1968, 1970; Tchalenko & Ambraseys, 1970). In these idealised models, rigid blocks are moved past each other, simulating strike-slip movement in a basement fault, with the clay/sand layer above representing a homogeneous, flat-lying cover sequence. A vertical Riedel shear zone forms in the clay/sand layer where strike-slip shear strain is imposed with slip surfaces developing in predictive geometries and with time sequences. Although the stratigraphy in the Dugald River deposit is steep and west-dipping, and currently there is no evidence to suggest a basement fault, there are field-based descriptions in the literature of Riedel shear zones that do not propagate from a basement fault (*e.g.* Mueller, 2020), or at the very least have not found evidence of a basement fault (*e.g.* Davis *et al.*, 2000). Furthermore, several publications describe Riedel shear zones for inclined to steeply dipping strata that have undergone folding (*e.g.* Dirks *et al.*, 2009, 2013; Mueller 2020; Swanson, 2006).

Within Riedel shear zones, fracture surfaces develop in distinctive geometric arrangements and are assigned terminology based on their kinematics and orientations (R, P, R′, P′, Y and T; Figure 13; *e.g.* Davis *et al.*, 2000; Passchier & Trouw, 2005; Riedel, 1929; Tchalenko, 1968). R- and P-shears develop synthetic to the shear direction, with Y-shears developed within the imposed shear direction. R′- and P′-shears are antithetic to the shear direction and are generally less well developed than synthetic shears, and R′-shears tend to develop in overlap zones between R-shears (Davis *et al.*, 2000). T-shears, or T-fractures, develop parallel to the principal stress direction (σ1) with extension parallel to the maximum instantaneous stretching axis (ISA1; Davis & Reynolds, 1996; Passchier & Trouw, 2005). Fractures within Riedel shear zones develop in an *en échelon* pattern (*e.g.* P-shears in Figure 13), and interconnecting segments (usually R′- and P-shears) develop an anastomosing pattern of shears that ultimately envelop lenses (Naylor *et al.*, 1986; Tchalenko, 1968). Evolved Riedel shear zones may result in the development of Y-shears, which, as displacement progresses, form throughgoing structures that 'wear' parallel to the bulk shear direction (here 259°/67°; Figure 14).

The geometric arrangement of fractures within a Riedel shear zone is defined by the angle at which a fracture occurs with respect to the bulk shear direction (*e.g.* Davis *et al.*, 2000; Tchalenko, 1970; Tchalenko & Ambraseys, 1970). This angle is described in terms of the internal friction angle (φ) of the deforming material relative to the shear direction. In a dextral Riedel shear zone, which is the case for the Dugald River Shear Zone, these are φ/2 for R-shears and 90–φ/2 for R′-shears in a clockwise direction to the shear zone. P-shears develop at φ/2,
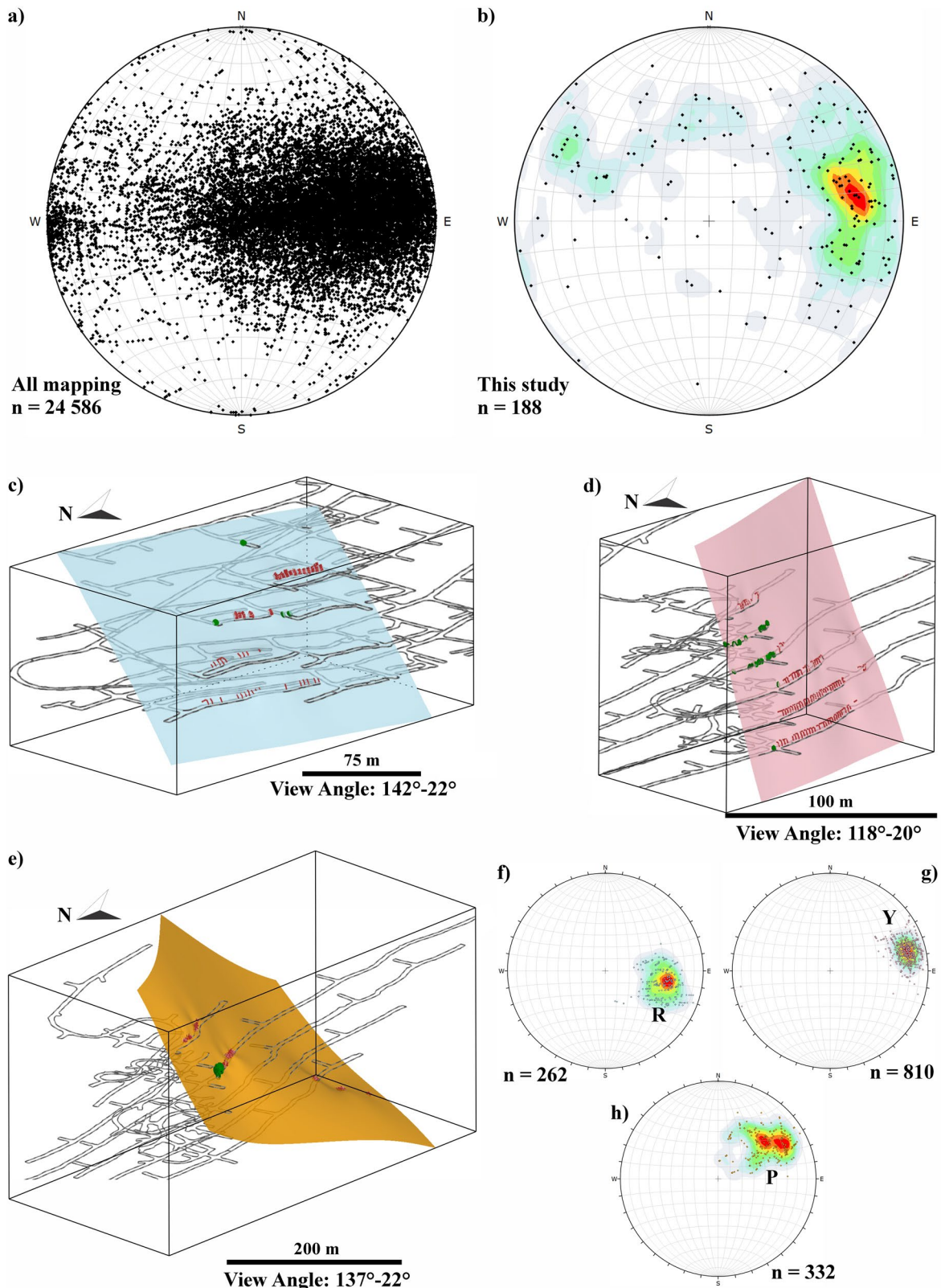
Figure 11. Modelling steps to differentiate populations on stereonets for poles to planes. (a) Poles to planes of faults, shears and fractures for all mapping data collected during this study [*viz.* face mapping (green discs) and digitising of virtual outcrops (maroon polylines)]. For digitised polylines, orientated vertices were extracted in order to plot on a stereonet. (b) Poles to planes of characterised mapping data of D_4-related structures (faults and shears) and classified as major or moderate during mapping indicating two broad populations centred at 260°/65° and 117°/77°. To differentiate the populations, surfaces were initially modelled in areas with high-density mapping data (c–e). The mapping data associated with the surfaces (f–h) revealed the distinctive pattern of a Riedel shear network (Figure 12). (c) R-shear and associated stereonet (f). (d) Y-shear with associated stereonet (g). (e) P-shear with associated stereonet (h).
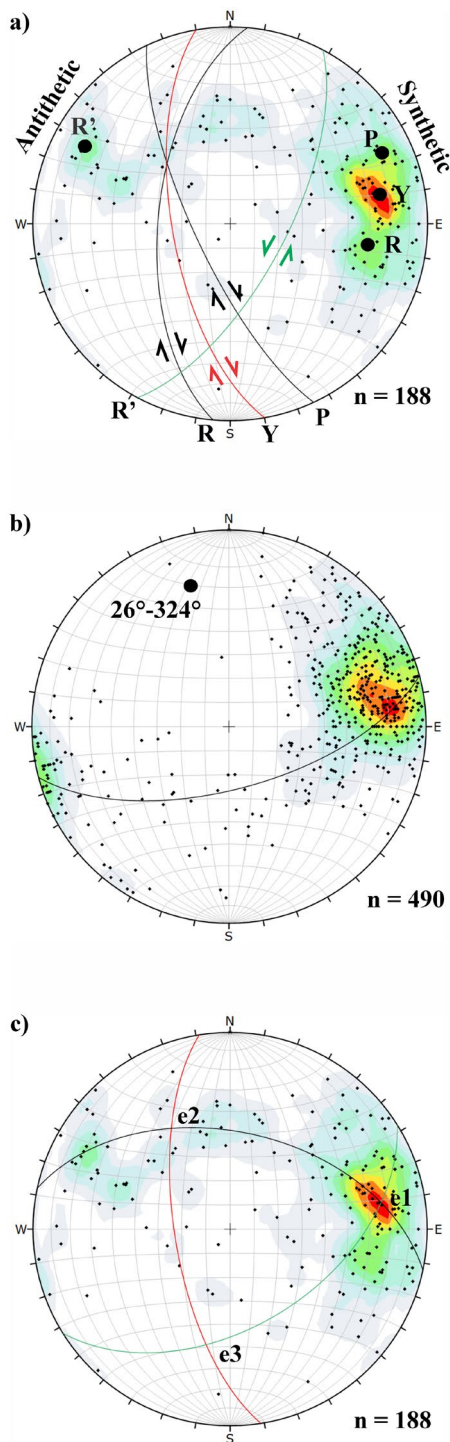
Figure 12. Equal area, lower-hemisphere stereoplots of poles to planes. Data were collected during underground face mapping and cover both the North and South Mine. Data used in the stereoplots are filtered to only include measurements with descriptive comments, particularly the scale of the structure measured. (a) Poles to D_4 shears (moderate and major scale) showing a distinctive Riedel shear network pattern. (b) Poles to S_0 and S_2. Synthetic shears plot within the same region as S_2 cleavage and indicate that D_2 and D_4 are co-planar. A best-fit girdle (26–324°) to poles of S_0 and S_2 indicates a gentle northwest plunge owing to D_4. (c) Poles to D_4 shears. Bingham statistics provide three eigenvalues, e1, e2 and e3. e1 at 23–081° provides a perpendicular modelling view that is parallel to the down-dip of the imposed shear direction (259/67°). e2 at 41–328° is parallel to the intermediate stretching axis defined by the plunges of inflections within steep, west-dipping shears and provides a localised trend for plunges within ore lenses. e3 at 41–192° is a useful vector, as releasing bends in the shear zone will occur along that trend.

and 90–φ/2 for P′-shears in an anticlockwise direction to the shear zone. Extensional T-fractures form at ~45° to the shear direction.

Brittle striations recorded on shear planes are inconclusive. This is in part due to the graphitic characteristic of the shear zone and the fact that graphite has a low friction coefficient and is suggested to have an important role in fault development as a 'lubricant' (*e.g.* Kirilova *et al.*, 2018; Rutter *et al.*, 2013). Another reason is that the anastomosing shear zone comprises multiple shear planes, including low-angle thrusts with a top-to-the-northeast sense of shear (*i.e.* dip-slip) that are prevalent in the South Mine. Nonetheless, observations in the North Mine suggest that most of the striations on the steep, west-dipping shears are subhorizontal, indicating predominately strike-slip movement in this part of the shear zone. In contrast, in the South Mine, striations also include dip-slip components along low-angle thrusts and steeper shear planes. The presence of both subhorizontal and subvertical striations along steep, D_4-related shears in the South Mine may be a result of initial strike-slip shear that rotated to dip-slip as the finite strain increased. However, more work will need to be done to confirm this.

Discussion

The structural analysis presented in this study, combined with dense drilling data and 3D modelling of the Dugald River Shear Zone, provides a unique opportunity to visualise how progressive deformation led to the development of an evolved Riedel shear zone with coeval high-grade Zn mineralisation. From the structural analysis and kinematic observations underground, it may be inferred that the Dugald River Shear Zone developed as a Riedel shear zone in a dextral, transpressional regime during D_4 of the Isan Orogeny (see Bell & Hickey, 1998; Creus *et al.*, 2023; O'Dea *et al.*, 1997; Spampinato *et al.*, 2015). During transpression, there is kinematic partitioning of simple shear parallel to the shear direction and coaxial flattening orthogonal to the shear zone (*e.g.* Dewey *et al.*, 1998; Fossen, 2010).

D_4 structural analysis

Several key values are derived from the structural analysis of D_4-related fractures and are presented on equal-area, lower-hemisphere stereonets of poles to planes (Figure 12). The majority of the D_4 shears plot within the same orientation as the pervasively developed S_2 fabric, reaffirming the co-planarity features formed during D_2 and D_4. Figure 12b shows a best-fit girdle to poles of S_0 and S_2, indicating a gentle northwest plunge owing to D_4, which is similar to the plunge observed in inflections in discrete shears and S-C′ lenses. The e1 eigenvalue derived from Bingham Statistics (Figure 12c) provides a viewing angle for modelling the Riedel shear zone, by providing an orientation of sectional views (slice plane) at 081°/23°; this is along the shear zones' dip direction and dip of 259°/67° (*e.g.* Figure 6).

Contoured maxima for synthetic R- and P-shears on stereonets show steep, west-to-southwest dips, while antithetic R′-shears have steep, southeast dips (Figure 12a). The acute
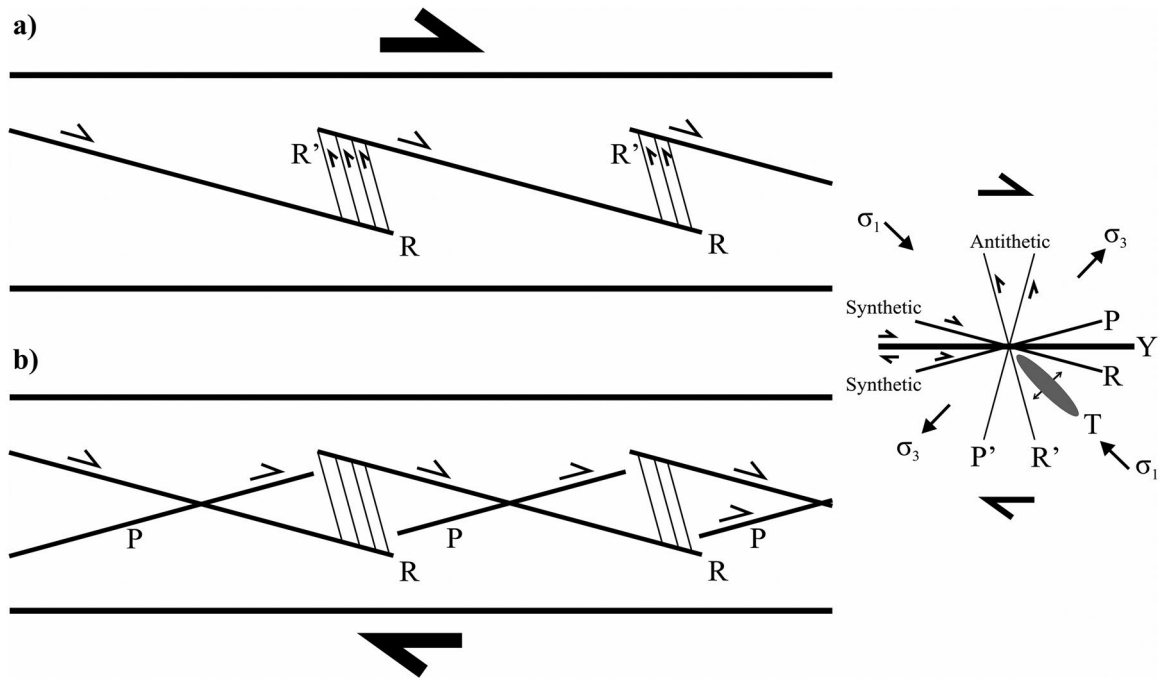
Figure 13. Steps 1 and 2 of Riedel shear zone development. (a) R-shears. These developed first, are the only criteria for a Riedel shear zone to develop and may have R'-shears developed in high compressive areas in overlap zones. At Dugald River Mine, R'-shears develop within overlap zones of R-shears and are characterised by discontinuous but thick shears with well-developed cataclastic fault cores. (b) P-shears. These developed when displacement along R-shears could no longer be sustained. Notably, R- and P-shear displacement occurs in a pulsating manner with local stress switching between R- and P-shear segments. Good examples of P-shears are observed along the footwall of the principal displacement zone within the long-term development of underground workings.
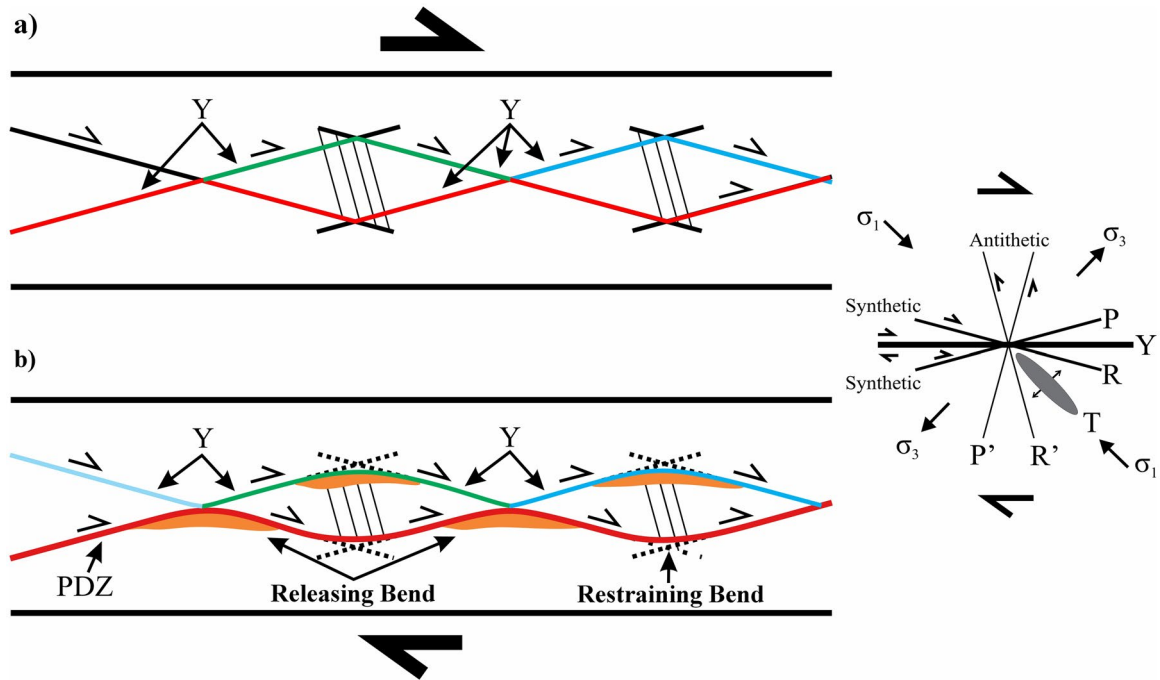
Figure 14. Steps 3 and 4 of Riedel shear zone development (also Figure 15). (a) Increasing displacement along R- and P-shears. This eventually resulted in segments terminating and overlapping with each other. At this stage, a throughgoing Y-shear developed and displacement propagated along it. Initially, the Y-shear had sharp segments, which wore down parallel to the bulk shear direction (b). Depending on the bend direction with respect to the bulk shear direction, a releasing or restraining bend may develop. In dextral shear zones, right-handed bends develop as dilational zones (orange polygons) and left-handed bends as contractional. (b) A Y-shear. This develops into a principal displacement zone, which then accommodates the bulk of the displacement. At Dugald River Mine, the principal displacement zone developed along the interface between a thick sulfide horizon and Dugald River Slates.
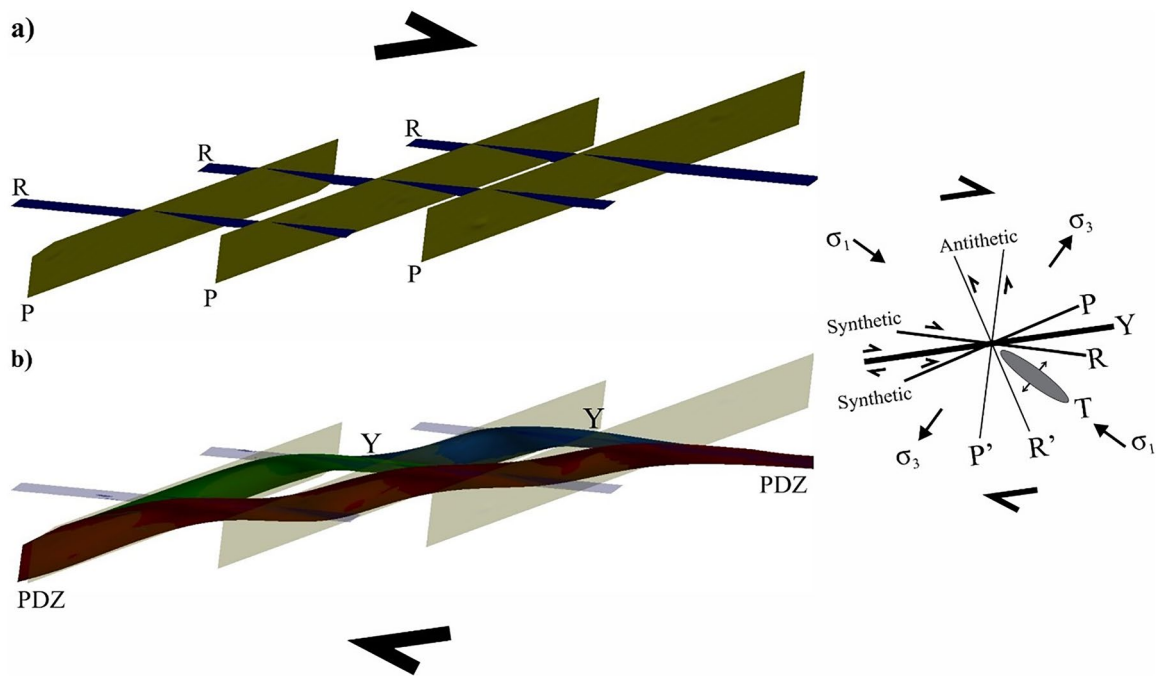
Figure 15. Idealised 3D representations to assist in visualising steps 3 (a) and 4 (b) of Riedel shear zone development. Surfaces were generated using the contoured maxima from stereonets (Figure 6) thus accurately representing the geometry of the R-, P- and Y- shears of the Dugald River Shear Zone, including the principal displacement zone (PDZ).

bisector, e3, at 40–198° (Figure 12c), of the contoured maxima for synthetic and antithetic structures, provides an important exploration vector, as it is subparallel to the bulk shear direction, and releasing bends may develop along that trend.

Development of the Dugald River Shear Zone

Pre-existing fabric

The detailed structural analysis in this study concludes that the Dugald River Shear Zone developed during D_4 brittle–ductile deformation. However, pre-existing fabric and competency contrast enacted a pivotal role in the position and development of the shear zones (see Everall & Sanislav, 2018; Sanislav et al., 2018). During the regional D_2 folding and with coeval development of axial planar cleavage, the stratigraphy in the Mount Roseby Corridor was rotated to subvertical orientations by isoclinal, overturned, east-verging folds with an associated well-developed axial planar cleavage (S_2; Creus et al., 2023; Newberry et al., 1993; Xu, 1996). The Dugald River Slates are less competent than the enveloping limestone to the east and the calc-silicate to the west (Figure 1a), and while all Mount Albert Group lithologies in the Mount Roseby Corridor were subjected to folding and cleavage development, the slates as a 'softer' or less competent unit preferentially accommodated strain via fold tightening and limb attenuation. The progressive fold tightening resulted in the formation of quartz–carbonate infill secondary accommodation structures such as flexural slip veining, layer-normal veins, hinge separation and boudinage along fold limbs of tighter folds (Creus et al., 2023). The development of

secondary accommodation structures during fold tightening was coeval with replacement of carbonate by sulfides and, in tighter folds, resulted in the interlinking of secondary accommodation structures, which Creus et al. (2023) refer to as Phase 1 mineralisation, resembling a crackle breccia, that was a preferential site for future high-strain zone development.

During D_3 orogenic collapse (Bell & Hickey, 1998; Creus et al., 2023; Davidson et al., 2002; Murphy, 2004; Xu, 1996), the principal compressive stress was subvertical, which resulted in the development of a subtle subhorizontal fabric. Of particular importance is the heterogeneous development of a crenulation cleavage that in the South Mine developed zones of S_3 intensification that locally rotated earlier fabrics to flatter, southwest dips. These zones were reactivated early during D_4 as low-angle thrust arrays with a top-to-the-east to -northeast displacement. Opposing shear along overlapping thrusts resulted in contractional and extensional sites, which promoted the remobilisation of sulfides and marked the onset of Phase 2 mineralisation (see Creus et al., 2023).

Early Phase 2 mineralisation is inferred to have occurred while the deposit was deforming through ductile means, and mineralisation continued while the deposit was exhumed through the brittle–ductile transition (Creus et al., 2023). We suggest that the result of this transition is that the rheological contrast that existed between the host slate and the pre-existing mineralisation produced strain-rate incompatibilities leading to the fracturing of the slate. The rheological stiffer or stronger slates had slower strain rates and combined with lower tensile strengths; the slates were prone to fracturing to accommodate the strain rate of the sulfide horizon. Notably, the

brittle–ductile transition is marked by the regional wrench tectonics that developed dextral strike-slip shears observed on regional maps (*e.g.* O'Dea *et al.*, 1997).

Increasing D_4 strain combined with the varying strain rate between the ductile-deforming sulfide horizon and the brittle-deforming slate resulted in the development of the Dugald River Shear Zone as a Riedel shear zone that we present in four steps:

1. initiation of simple shear resulting in the development of the R-shears, and R′-shears within overlap zones between R-shears;
2. increasing displacement along R-shears resulting in the development of P-shears;
3. interconnection between R- and P-shears developed into throughgoing Y-shears; and
4. eroding of Y-shears into parallelism with the shear direction where R- and P-shears connected to form the Y-shears; development of a principal displacement zone that accommodated the bulk of the stress.

The following section discusses the four-step development of the Dugald River Shear Zone in more detail. The first three steps are inferred to be associated with mostly mechanical remobilisation of sulfides on the scale of tens of metres, whereas the fourth step is inferred to be associated with significant enrichment migration of sulfides from depth through high-permeability Y-shears, in the concentration of sulfides via mixed-state solution (see Creus *et al.*, 2023). The Dugald River Shear Zone effectively represents a high-permeability channel way that was enveloped by impermeable slates, while dilational sites proximal to the shear zone were preferential sites for sulfide accumulation.

At Dugald River Mine, Y-shears are well developed in the southern part of the deposit and are inferred to have been largely driven by the presence of a thick sulfide horizon that acted as a weak horizon within the host slate and provided an ideal site for focused strain partitioning, which coupled with zones of S_3 intensification that were reactivated as low-angle thrust lenses during early D_4 (see Creus *et al.*, 2023). Consequently, in the southern part of the deposit, the shear zone has numerous anastomosing shears developed at all scales (Figure 5). Thus, while a mapping point may suggest a P-shear, the shear plane may 'bend' into the imposed shear direction within the rock mass and further along strike 'bend' into a general R-shear direction; this makes modelling complex anastomosing shear zones using dense 3D data intricate. The anastomosing nature of the shears resulted in numerous, multi-scale releasing and restraining bends while maintaining steep dips. Consequently, releasing bends provided ideal sites for syntectonic sulfide remobilisation and subsequent high-grade Zn brecciation during D_4 (Creus *et al.*, 2023).

Step 1: R- and R′-shears

The first step is inferred to have occurred owing to incompatible strain rates between the sulfide horizon and slates. The first shears that developed were R-shears that are synthetic with respect to the bulk shear direction (Figure 13a) and have a contoured maxima of poles to planes on stereonets of 281°/61° (Figure 12a). In the overlap zones of R-shears, R′-shears developed owing to the high compressive stress that occurs in these zones (*e.g.* Davis *et al.*, 2000) and have a contoured maxima of poles to planes on stereonets of 117°/77° (Figure 12a). At Dugald River Mine, the development of R′-shears in the overlap zones appears to have been heterogeneous, and given the available data, we suggest that the South Mine represents an overlap between at least two R-shears and the North Mine between another two. Furthermore, we suggest that the heterogeneous development of R′-shears in the South Mine was due to the low-angle thrust arrays continuing to develop with the Riedel shear zone, which would have compounded the compressive stress in the overlap zones between R-shears, in contrast to the North Mine where fewer R′-shears have developed. Low-angle thrusts, combined with the development of R′-shears in the South Mine, are an important structural control on Phase 2 mineralisation, as this created additional opposing and converging slip planes that further promoted sulfide remobilisation.

Step 2: P-shears

The increasing D_4 strain resulted in R-shear growth that reached a point where shears were unfavourably orientated to sustain large relative displacements (*e.g.* Tchalenko, 1970) and P-shears developed to accommodate the strain (Figure 13b). Good examples of P-shears are observed in the footwall development where macro-scale discrete shears have been modelled (*e.g.* Figure 6) with a consistent spacing of ~350m. The P-shears are synthetic to the dextral shear direction and created additional dilation sites, albeit not as effective as the combination of low-angle thrusts and R′-shears prevalent in the South Mine. However, as the P-shears developed *en échelon*, at a regular spacing, in response to the rotation of the local principal stress (*e.g.* Tchalenko, 1970), their distribution became widespread or more prominent within the shear zone and promoted mechanical remobilisation of sulfides at a local scale, particularly where they intersected R-shears.

Step 3: Y-shears

In evolved Riedel shear networks, throughgoing shears (Y-shears) develop by interconnected R- and P-shear segments (Figures 14a and 15a). Early development of Y-shears produced sharp angles at merger points of R- and P-shears (Figures 14a and 15a), and with progressive development, these start to wear parallel to the bulk shear direction (Figures 14b and 15b), involving modification through both abrasive and adhesive wear. Abrasive wear results in cataclastic core growth, brecciation and gouge development, and adhesive wear results in sidewall rip-out that creates asymmetric lenses of wall rock (Swanson, 2005, 2006). At Dugald River Mine, these zones are represented by high-strain zones with a well-developed S-C′ fabric (*e.g.* Figure 10a), with the S- and C′-planes parallel to R- and P-shears, respectively. Abrasive wear is responsible for the development of cataclastic fault cores, reactivated during late D_5 brittle deformation to form incohesive cataclasites and fault breccia. Furthermore, the sidewall rip-outs pose a geotechnical concern, as they will have developed at the scale of stopes along with numerous small-scale shears that combined may result in breakout of stope walls to development level-scale Y-shears (Figure 16).
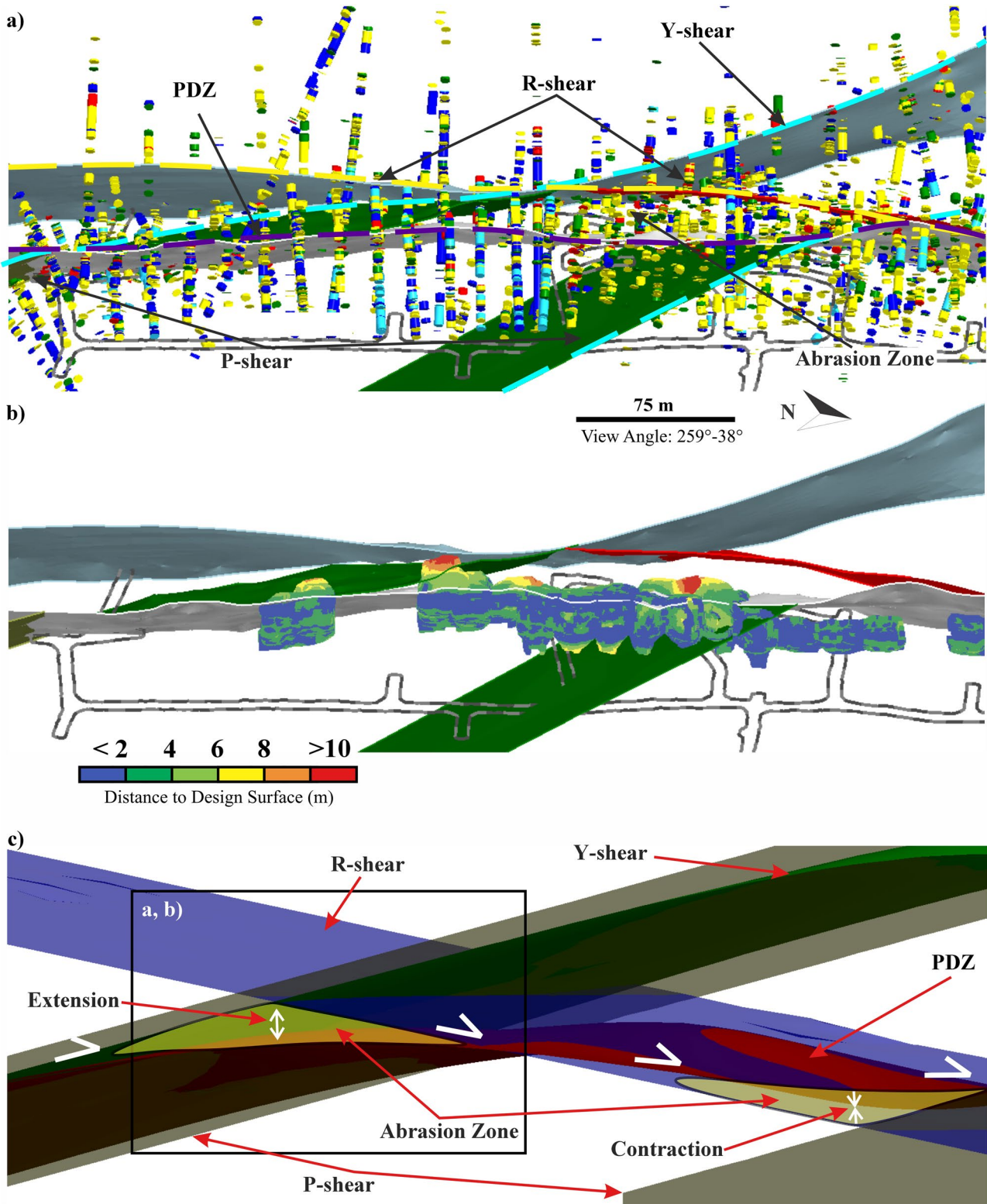
Figure 16. Riedel shear zone development. As the development progresses progresses, R- and P-shear segments merge to form throughgoing Y-shears. (a) At Dugald River Mine, the terminations of R- and P-shears eroded to form zones of abrasion that, when drilled through, are marked by numerous intersections that are difficult to link or assign to discrete shears. Furthermore, the intervals comprise fault cores of cataclasite and fault breccia. (b) View of the S340 stope voids in the South Mine showing the distance of the void walls to the design surface. Zones of abrasion are of geotechnical concern, as stopes that are designed in these zones are subject to overbreak. (c) Idealised 3D representation of the eroding of R- and P- shear termination zones to develop Y-shears. This also results in the development of abrasion zones. Half arrows indicate the propagation direction of the principal displacement zone (PDZ) that may develop into an extensional and contractional zone.

Step 4: principal displacement zone

During the final step, most of the strain was accommodated along Y-shears, which progressively widened, with one of the Y-shears developed into a principal displacement zone (Figures 14b and 15b). At Dugald River Mine, the principal displacement zone developed along the hanging wall of a strike-extensive, continuous sulfide horizon. Y-shears are common to the west of the principal displacement zone and bifurcate and merge with it (Figure 5). The principal displacement zone represents a continuous high-permeability channel way through which sulfides migrated and dilational zones developed along the structure (Figure 14). At Dugald River Mine, the dilational zones are responsible for high-grade Zn breccia ore in the South Mine as well as hanging wall lenses that occur along the footwall of other major Y-shears like the Patties Shear (Figure 14).

Predictive 3D modelling

In the mining industry, 3D models form the basis for safe and optimised mining forming a pivotal role in reducing operational risk. Thus, in geologically complex deposits, close drill-hole spacing may be required to confirm geological and grade continuity resulting in dense data. However, in deposits such as that at the Dugald River Mine, which are hosted by anastomosing shear zones with significant damage zones, successful or confident recording of orientated measurements from drill core may be variable, as drill core may routinely fail orientation criterion. Thus, regular collection of mapping data is vital in ensuring that a high-quality 3D model is constructed and routinely updated.

The *en échelon* characteristic of Riedel shear networks allows for predictive modelling from both a resource definition and geotechnical perspective. The Dugald River Shear Zone represents an evolved Riedel shear zone with well-developed Y-shears, which allows for predicting localised areas that were under contraction or extension, *i.e.* dilational zones in the form of restraining and releasing bends along the throughgoing Y-shears (Figures 17 and 19).

The volumes of contraction and extension are governed by the intersection of P-shear with R-shear segments with respect to the bulk dextral shear sense of the Dugald River Shear Zone, while Y-shears continued to develop. The development of restraining and releasing bends is governed by the propagation of the Y-shears as they develop and as displacement continued (*e.g.* Figure 16c). Figure 17 is a series of depth slices through the deposit, highlighting how releasing bends developed along throughgoing structures. Releasing bends developed where a throughgoing Y-shear propagated from a P-shear to an R-shear
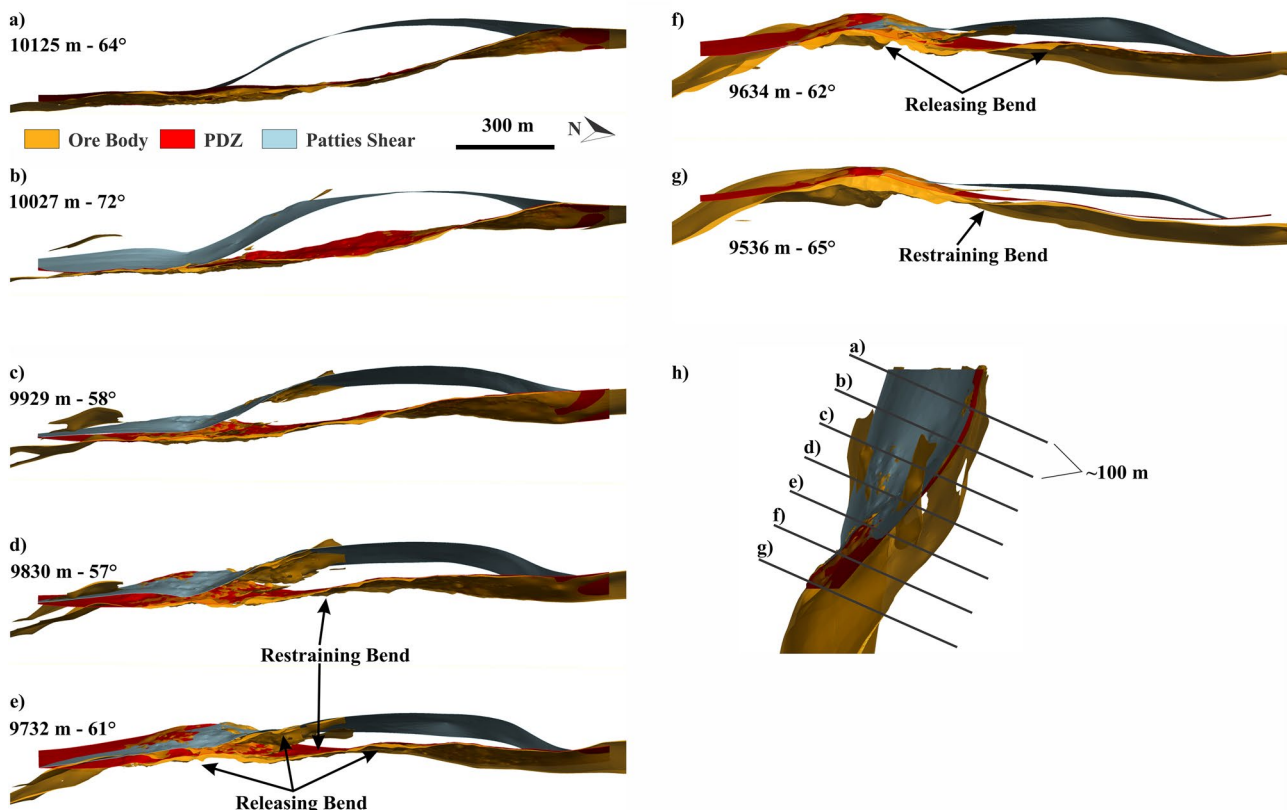
Figure 17. Depth sections through the Dugald River Shear Zone with the high-grade ore volume. The ore volume was provided by Dugald River Mine and was current as of December 2020. The depth of each section is in the mine grid coordinate system, and the location of each slice is shown in (h). The view angle for each section accounts for the curvi-planar character of the shear zone, to ensure that each section has a down-dip view of the principal displacement zone. Releasing and restraining bends are best illustrated towards the lower levels of the mine where the flexure in the shear zone is best developed (*e.g.* d–f).
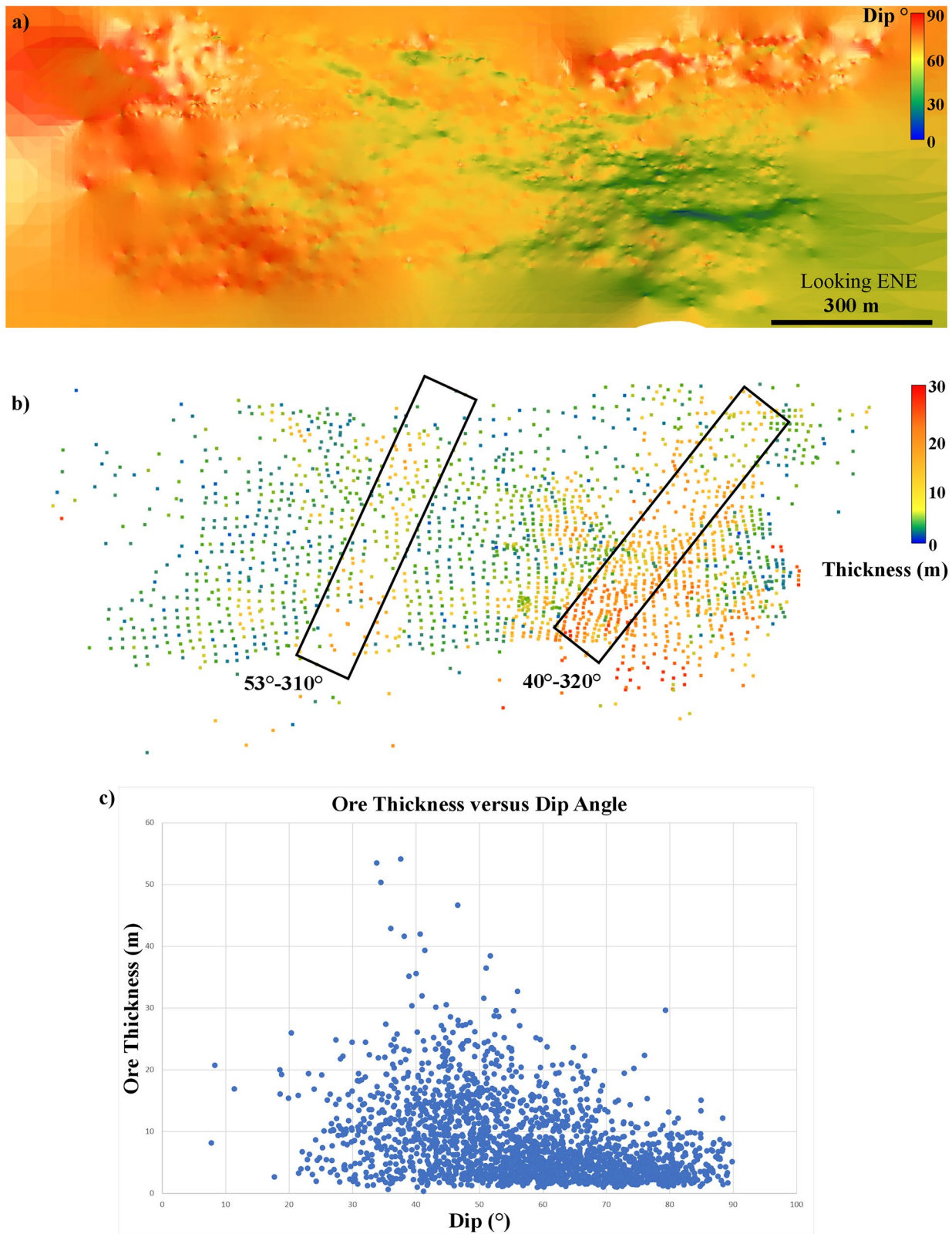
Figure 18. (a) East-northeast view of the principal displacement zone with the face dip of interconnected triangles colour-coded according to dip angle. The Dugald River Shear Zone geometry is mirrored by the principal displacement zone and is steeper to the north and towards the surface. The flexure in the South Mine is illustrated by a lower dip angle for the shear zone and owing to zones of S_3 intensification that were reactivated as low-angle thrust arrays during D_4. Remnant P-shear segments towards the east of the principal displacement zone were reactivated during D_5, together with the low-angle thrusts and locally segmented the shear zone and ore body, as illustrated by localised lower angle dips. (b) Interval midpoints for drilling data used to generate the high-grade Zn wireframe volume provided by Dugald River Mine. Only intervals for the main ore lens that occurs along the footwall of the principal displacement zone are shown with the true thickness of the ore lens at a respective point calculated and colour-coded. In general, the ore body is thicker where there are lower dip angles, as indicated in the scatter plot (c), and this supports the conclusion by Ford *et al.* (2009) that maximum dilation occurs at ~45° dip angles for faults. The e2 value, from the stereoplots (Figure 6c), can be used as a localised exploration vector for trends in the ore lenses as indicated by the black boxes in (b).
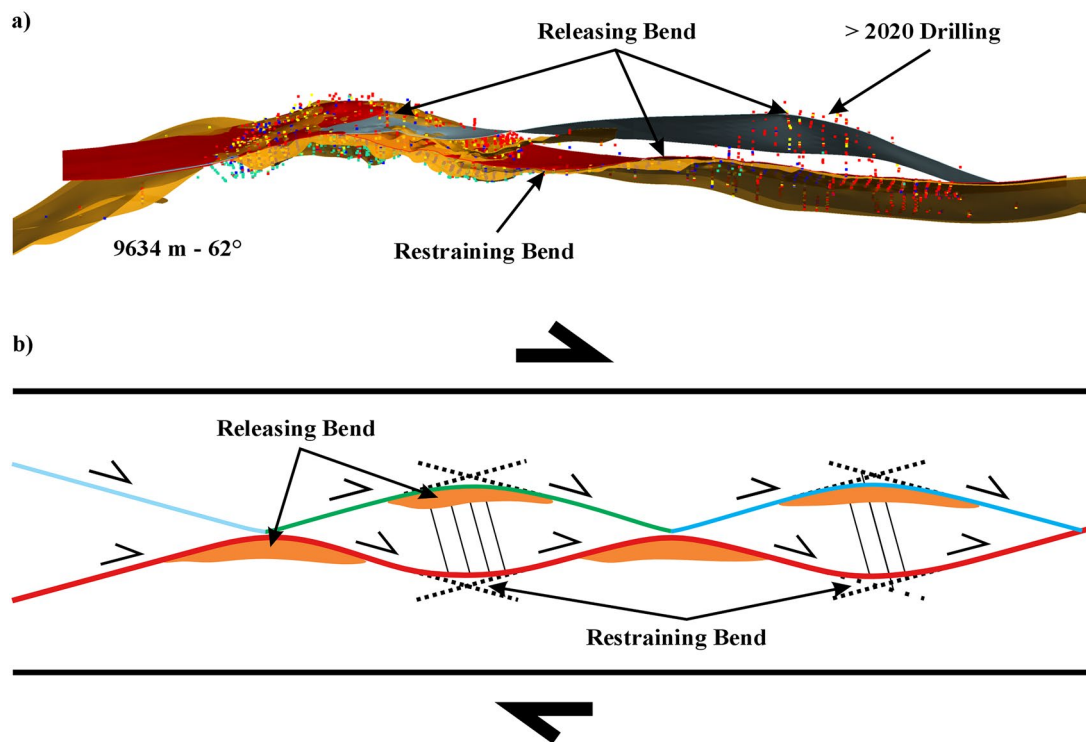
Figure 19. (a) Down-dip view of the Dugald River Shear Zone. Included are the principal displacement zone and Patties Shear modelled for this study, applying a data cutoff of December 2019; the high-grade Zn wireframe volume of December 2020 (provided by Dugald River Mine); and logged intervals for ore textures up to November 2021. (b) Idealised model of a dextral Riedel shear network showing where releasing and restraining bends may form as Y-shears propagate during development. High-resolution 3D modelling of the Dugald River Shear Zone allows the release of bends in the shear zone to be predicted and therefore sites for targeted drilling campaigns.

and further along the R-shear to create a right-handed bend in the Y-shear (*e.g.* Figures 14b, 15b, 16c, and 17d–g), whereas restraining bends developed where a throughgoing Y-shear propagated along an R-shear to a P-shear and further along the P-shear to create a left-handed bend in the Y-shear (*e.g.* Figures 14b, 15b, and 17d, e, g). In dextral shears, right-handed bends and jogs are dilational, whereas left-handed bends and jogs are compressional (Blenkinsop, 2000). Releasing bends may be expected where drilling intersects north-northwest-trending shears with north-trending shears to the north. In contrast, restraining bends may be expected where drilling intersects north-northwest-trending shears with north-trending shears to the south. Lastly, releasing bends may occur along the e3 direction, which in the case of the Dugald River Shear Zone is 41–192° (Figure 12c).

The positions of lenses of high-grade Zn mineralisation within the Dugald River Shear Zone can be predicted based on the geometry of the Y-shears. Where the shear zone is steep, thick, high-grade Zn lenses are unlikely to occur, as the shear zone was near orthogonal to the subhorizontal west-south-west–east-northeast shortening direction, and coaxial deformation dominated to produce transposition-related Phase 2 mineralisation (Figure 17a–c). Ford *et al.* (2009) observed that maximum dilation occurred in faults with a dip angle of ~45°, which at Dugald River Mine occurs in the South Mine, as indicated by the thickest part of the ore body, and the shear zone dips at around 45° (Figures 8 and 18). Thus, the South Mine represents a macro-scale releasing bend expressed by the

development of a thick sulfide lens within a right-handed bend of the principal displacement zone (Figures 17f and 19). Subordinate lenses have developed from this thick sulfide lens along Y-shears, with releasing and restraining bends developing (Figures 17d, e and 19).

The predictive character of Riedel shear networks and their use in exploration vectoring are illustrated in Figure 19. The data cutoff for the 3D modelling in this study was December 2019, and included in Figure 19 is the high-grade Zn volume for December 2020 as well as the logged ore textures from drilling up to November 2021. The Y-shear to the west (*i.e.* Patties Shear) was constructed as bifurcating towards the north-northeast from the principal displacement zone, using high-confidence drilling and mapping data available at the time. Based on observations from underground mapping, limited surface drilling and subsequent 3D modelling, the Y-shear was modelled to 'merge back' into the principal displacement zone towards the north. By undertaking a detailed structural analysis (*i.e.* Figure 12), concluding that the shear zone developed as a Riedel shear network and applying a comprehensive understanding of the 3D geometry of Riedel shear zones, a releasing bend was modelled and confirmed with post-data cutoff drilling (Figure 19).

Conclusions

Analysis of structures and mineralisation along the Dugald River Shear Zone provides insights into the relationship between

mineralisation and dilational sites that are created within an anastomosing Riedel shear zone as it develops. The structural complexity of the shear zone necessitates dense drilling and, combined with high-grade Zn ore lenses occurring along the footwall of continuous Y-shears, results in a robust dataset of drilling and mapping data, including virtual outcrops from SfM-MVS. A high-resolution 3D model of the shear zone was constructed; this serves to highlight existing areas of dilation (*i.e.* releasing bends, *e.g.* Figures 14b, 15b, 16c, 17, and 19) as well as being predictive when extrapolating shears into areas of sparse data (*e.g.* Figure 19). Furthermore, within active mining fronts, contractional zones (*i.e.* restraining bends; Figure 16) that developed within the shear zones can also be predicted and used to mitigate risk.

The main outcomes from the study are as follows:

- The geometry of the Riedel shear zone determines the distribution of the ore lenses and their thickness. The ore is thickest within right-handed bends within through-going shears and where the shear zone has a ~45° dip.
- The *en échelon* characteristic of Riedel shear zones means that dilational and compressive zones within the shear zone can be predicted and allow for targeted drilling along the e3 (41–192°) direction, which is determined from a structural analysis of D_4-related fabric.

The robust drilling data combined with mapping data provide an ideal case study of how dense structural data can be interpreted, which can subsequently be extended to 3D modelling and exploration vectoring. With a robust understanding of the structural framework and geometry of a shear zone, predictive modelling can be applied to determine where additional releasing bends may occur within a shear zone and therefore where the highest grades and thickest intervals of mineralisation may potentially be found. Ultimately this leads to increased ore-body knowledge, lowering of drilling costs, and extending the life of the asset.

ORCID

P. K. Creus http://orcid.org/0000-0002-8695-3675
I. V. Sanislav http://orcid.org/0000-0002-3680-3740
P. H. G. M. Dirks http://orcid.org/0000-0002-1582-1405

Data availability statement

Owing to the nature of the research [with ethical/legal/commercial constraints] supporting data not included within this paper are not available.

References

Abu Sharib, A. S. A. A., & Bell, T. H. (2011). Radical changes in bulk shortening directions during orogenesis; significance for progressive development of regional folds and thrusts. *Precambrian Research*, *188*(1-4), 1–20. https://doi.org/10.1016/j.precamres.2011.03.008

Abu Sharib, A. S. A. A., & Sanislav, I. V. (2013). Polymetamorphism accompanied switching in horizontal shortening during Isan Orogeny; Example from the Eastern Fold Belt, Mount Isa Inlier, Australia. *Tectonophysics*, *587*, 146–167. https://doi.org/10.1016/j.tecto.2012.06.051

Arboleya, M. L., & Engelder, T. (1995). Concentrated slip zones with subsidiary shears; their development on three scales in the Cerro Brass fault zone, Appalachian Valley and Ridge. *Journal of Structural Geology*, *17*(4), 519–532. https://doi.org/10.1016/0191-8141(94)00079-F

Barcos, L., Díaz-Azpiroz, M., Balanyá, J. C., Expósito, I., Jiménez-Bonilla, A., & Faccenna, C. (2016). Analogue modelling of inclined, brittle–ductile transpression; testing analytical models through natural shear zones (external Betics). *Tectonophysics*, *682*, 169–185. https://doi.org/10.1016/j.tecto.2016.05.021

Basson, I. J., Creus, P. K., Anthonissen, C. J., Stoch, B., & Ekkerd, J. (2016). Structural analysis and implicit 3D modelling of high-grade host rocks to the Venetia kimberlite diatremes, Central Zone, Limpopo Belt, South Africa. *Journal of Structural Geology*, *86*, 47–61. https://doi.org/10.1016/j.jsg.2016.03.002

Basson, I. J., Lourens, P., Paetzold, H-D., Thomas, S., Brazier, R., & Molabe, P. (2017). Structural analysis and 3D modelling of major mineralizing structures at the Phalaborwa copper deposit. *Ore Geology Reviews*, *83*, 30–42. https://doi.org/10.1016/j.oregeorev.2016.12.002

Basson, I. J., McCall, M. J., Andrew, J., & Daweti, E. (2018). Structural controls on mineralisation at the Namib lead and zinc mine, Damara Belt, Namibia. *Ore Geology Reviews*, *95*, 931–944. https://doi.org/10.1016/j.oregeorev.2018.03.028

Basson, I. J., Thomas, S. A. J., Stoch, B., Anthonissen, C. J., McCall, M. J., Britz, J., Macgregor, S., Viljoen, S., Nel, D., Vietze, M., Stander, C., Horn, J., Bezuidenhout, J., Sekoere, T., Gous, C., & Boucher, H. (2018). The structural setting of mineralisation at Kolomela Mine, Northern Cape, South Africa, based on fully-constrained, implicit 3D modelling. *Ore Geology Reviews*, *95*, 306–324. https://doi.org/10.1016/j.oregeorev.2018.02.032

Bell, T. H. (1983). Thrusting and duplex formation at Mount Isa, Queensland, Australia. *Nature (London)*, *304*(5926), 493–497. https://doi.org/10.1038/304493a0

Bell, T. H. (1991). The role of thrusting in the structural development of the Mount Isa Mine and its relevance to exploration in the surrounding region. *Economic Geology*, *86*(8), 1602–1625. https://doi.org/10.2113/gsecongeo.86.8.1602

Bell, T. H., & Hickey, K. A. (1998). Multiple deformations with successive subvertical and subhorizontal axial planes in the Mount Isa region; their impact on geometric development and significance for mineralization and exploration. *Economic Geology*, *93*(8), 1369–1389. https://doi.org/10.2113/gsecongeo.93.8.1369

Bell, T. H., Reinhardt, J. W., & Hammond, R. L. (1992). Multiple foliation development during thrusting and synchronous formation of vertical

shear zones. *Journal of Structural Geology*, *14*(7), 791–805. https://doi.org/10.1016/0191-8141(92)90041-T

Betts, P. G., Giles, D., Mark, G., Lister, G. S., Goleby, B. R., & Aillères, L. (2006). Synthesis of the Proterozoic evolution of the Mt Isa Inlier. *Australian Journal of Earth Sciences*, *53*(1), 187–211. https://doi.org/10.1080/08120090500434625

Blake, D. H. (1987). *Geology of the Mount Isa Inlier and environs, Queensland and Northern Territory*. Bureau of Mineral Resources Bulletin 225, 83p.

Blake, D. H., & Stewart, A. J. (1992). Stratigraphic and tectonic framework, Mount Isa Inlier. In A. J. Stewart & D. H. Blake (Eds.), *Detailed studies of the Mount Isa Inlier* (pp. 1–11). Australian Geological Survey Organisation, Bulletin 243. https://ecat.ga.gov.au/geonetwork/srv/api/records/a05f7892-9cf8-7506-e044-00144fdd4fa6

Blenkinsop, T. G. (2000). *Deformation microstructures and mechanisms in minerals and rocks*. Kluwer Academic Publishers.

Carson, C. J., Hutton, L. J., Withnall, I. W., & Perkins, W. G. (2009). *Joint GSQ-GA NGA geochronology project, Mount Isa region, 2007–2008*. Queensland Geological Record 2008/05.

Carson, C. J., Hutton, L. J., Withnall, I. W., Perkins, W. G., Donchak, P. J. T., Parsons, A., Blake, P. R., Sweet, I. P., Neumann, N. L., & Lambeck, A. (2011). *Summary of results: Joint GSQ-GA NGA geochronology project, Mount Isa Region, 2009–2010*. Queensland Geological Record 2011/03.

Cawood, A. J., Bond, C. E., Howell, J. A., Butler, R. W. H., & Totake, Y. (2017). LiDAR, UAV or compass-clinometer? Accuracy, coverage and the effects on structural models. *Journal of Structural Geology*, *98*, 67–82. https://doi.org/10.1016/j.jsg.2017.04.004

Chemenda, A. I., Cavalié, O., Vergnolle, M., Bouissou, S., & Delouis, B. (2015). Numerical model of formation of a 3-D strike-slip fault system. *Comptes Rendus. Géoscience*, *348*(1), 61–69. https://doi.org/10.1016/j.crte.2015.09.008

Cho, N., Martin, C. D., & Sego, D. C. (2008). Development of a shear zone in brittle rock subjected to direct shear. *International Journal of Rock Mechanics and Mining Sciences*, *45*(8), 1335–1346. https://doi.org/10.1016/j.ijrmms.2008.01.019

Cowan, E. J., Beatson, R., Ross, H. J., Fright, W. R., McLennan, T. J., Evans, T. R., Carr, J. C., Lane, R. G., Bright, D. V., Gillman, A. J., Oshust, P. A., & Titley, M. (2003). Practical implicit geological modelling. In S. Dominy (Ed.), *Fifth International Mining Geology Conference Proceedings*. (Vol. 8/2003, pp. 89–99). The Australasian Institute of Mining and Metallurgy.

Creus, P. K. (2022). *3D structural controls of the shear zone hosted Dugald River zinc-lead-silver deposit, Mount Isa Inlier, Australia* [Unpublished PhD thesis]. James Cook University. https://doi.org/10.25903/9x7f-jw34

Creus, P. K., Basson, I. J., Koegelenberg, C. K., Ekkerd, J., de Graaf, P. J. H., Bester, M., & Mokele, T. (2019). 3D fabric analysis of Venetia Mine, South Africa; using structural measurements and implicitly-modelled surfaces for improved pit slope design and risk management. *Journal of African Earth Sciences*, *155*, 137–150. https://doi.org/10.1016/j.jafrearsci.2019.04.009

Creus, P. K., Basson, I. J., Stoch, B., Mogorosi, O., Gabanakgosi, K., Ramsden, F., & Gaegopolwe, P. (2018). Structural analysis and implicit 3D modelling of Jwaneng Mine; insights into deformation of the Transvaal Supergroup in SE Botswana. *Journal of African Earth Sciences*, *137*, 9–21. https://doi.org/10.1016/j.jafrearsci.2017.09.010

Creus, P. K., Sanislav, I. V., & Dirks, P. H. G. M. (2021). Application of SfM-MVS for mining geology: Capture set-up and automated processing using the Dugald River Zn-Pb-Ag mine as a case study. *Engineering Geology*, *293*, 106314. https://doi.org/10.1016/j.enggeo.2021.106314

Creus, P. K., Sanislav, I. V., Dirks, P. H. G. M., Jago, J. M., & Davis, B. K. (2023). The Dugald River-type, shear zone hosted, Zn-Pb-Ag mineralisation, Mount Isa Inlier, Australia. *Ore Geology Reviews*, *155*, 105369. https://doi.org/10.1016/j.oregeorev.2023.105369

Davidson, G. J., Davis, B. K., & Garner, A. (2002). Structural and geochemical constraints on the emplacement of the Monakoff Oxide Cu-Au(-Co-U-REE-Ag-Zn-Pb) deposit, Mt Isa Inlier, Australia. In T. M. Porter (Ed.), *Hydrothermal iron oxide copper-gold & related deposits: A global perspective* (pp. 49–75). PGC Publishing.

Davis, B. K. (2017). *Dugald River – Orebody Knowledge Study (DROKS)*. Unpublished report by Orefind.

Davis, G. H., Bump, A. P., García, P. E., & Ahlgren, S. G. (2000). Conjugate Riedel deformation band shear zones. *Journal of Structural Geology*, *22*(2), 169–190. https://doi.org/10.1016/S0191-8141(99)00140-6

Davis, G. H., & Reynolds, S. J. (1996). *Structural geology: Of rocks and regions* (2nd ed.). John Wiley.

Dewey, J. F., Holdsworth, R. E., & Strachan, R. A. (1998). Transpression and transtension zones. In R. E. Holdsworth, R. A. Strachan, & J. F. Dewey (Eds.), *Continental transpressional and transtensional tectonics* (pp. 1–14). Geological Society Special Publications, 135(1). https://doi.org/10.1144/GSL.SP.1998.135.01.01

Dirks, P. G. H. M., Charlesworth, E. G., & Munyai, M. R. (2009). Cratonic extension and Archaean gold mineralisation in the Sheba-Fairview mine, Barberton Greenstone Belt, South Africa. *South African Journal of Geology*, *112*(3-4), 291–316. https://doi.org/10.2113/gssajg.112.3-4.291

Dirks, P. H. G. M., Charlesworth, E. G., Munyai, M. R., & Wormald, R. (2013). Stress analysis, post-orogenic extension and 3.01 Ga gold mineralisation in the Barberton greenstone belt, South Africa. *Precambrian Research*, *226*, 157–184. https://doi.org/10.1016/j.precamres.2012.12.007

Everall, T., & Sanislav, I. V. (2018). The influence of pre-existing deformation and alteration textures on rock strength, failure modes and shear strength parameters. *Geosciences*, *8*(4), 124. https://doi.org/10.3390/geosciences8040124

Ford, A., Blenkinsop, T. G., & McLellan, J. G. (2009). Factors affecting fluid flow in strike-slip fault systems: Coupled deformation and fluid flow modelling with application to the western Mount Isa Inlier, Australia. *Geofluids*, *9*(1), 2–23. https://doi.org/10.1111/j.1468-8123.2008.00219.x

Fossen, H. (2010). *Structural geology*. Cambridge University Press.

Foster, D. R. W., & Austin, J. (2008). The 1800–1610 Ma stratigraphic and magmatic history of the Eastern Succession, Mount Isa Inlier, and correlations with adjacent Paleoproterozoic terranes. *Precambrian Research*, *163*(1-2), 7–30. https://doi.org/10.1016/j.precamres.2007.08.010

Foster, D. R. W., & Rubenach, M. J. (2006). Isograd pattern and regional low-pressure, high-temperature metamorphism of pelitic, mafic and calc-silicate rocks along an east–west section through the Mt Isa Inlier. *Australian Journal of Earth Sciences*, *53*(1), 167–186. https://doi.org/10.1080/08120090500434617

Gibson, G. M., Meixner, A. J., Withnall, I. W., Korsch, R. J., Hutton, L. J., Jones, L. E. A., Holzschuh, J., Costelloe, R. D., Henson, P. A., & Saygin, E. (2016). Basin architecture and evolution in the Mount Isa mineral province, northern Australia; constraints from deep seismic reflection profiling and implications for ore genesis. *Ore Geology Reviews*, *76*, 414–441. https://doi.org/10.1016/j.oregeorev.2015.07.013

Giles, D., Betts, P. G., Aillères, L., Hulscher, B., Hough, M., & Lister, G. S. (2006). Evolution of the Isan Orogeny at the southeastern margin of the Mt Isa Inlier. *Australian Journal of Earth Sciences*, *53*(1), 91–108. https://doi.org/10.1080/08120090500432470

Grose, L., Ailleres, L., Laurent, G., & Jessell, M. (2021). LoopStructural 1.0: Time-aware geological modelling. *Geoscientific Model Development*, *14*(6), 3915–3937. https://doi.org/10.5194/gmd-14-3915-2021

Harris, P. (2015). Dugald River case study – The importance of understanding your orebody and designing your mine for maximum value. In Y. Polvin (Ed.), *Underground design methods* (pp. 21–36). Australian Centre for Geomechanics. https://doi.org/10.36487/ACG_rep/1511_0.2_Harris

Hill, E. V., Oliver, N. H. S., Cleverley, J. S., Nugus, M. J., Carswell, J., & Clark, F. (2014). Characterisation and 3D modelling of a nuggety, vein-hosted gold ore body, Sunrise Dam, Western Australia. *Journal of Structural Geology*, *67*, 222–234. https://doi.org/10.1016/j.jsg.2013.10.013

Hillacre, S., Ansdell, K., & McEwan, B. (2021). Geology, structural analysis, and paragenesis of the Arrow uranium deposit, western Athabasca Basin, Saskatchewan, Canada; implications for the development of the Patterson Lake corridor. *Economic Geology*, *116*(2), 285–321. https://doi.org/10.5382/econgeo.4797

Hillier, M. J., Schetselaar, E. M., de Kemp, E. A., & Perron, G. (2014). Three-dimensional modelling of geological surfaces using generalized interpolation with radial basis functions. *Mathematical Geosciences*, *46*(8), 931–953. https://doi.org/10.1007/s11004-014-9540-3

Hobbs, B. E. (1987). Principles involved in mobilization and remobilization. *Ore Geology Reviews*, *2*(1-3), 37–45. https://doi.org/10.1016/0169-1368(87)90022-9

Jackson, M. J., Scott, D. L., & Rawlings, D. J. (2000). Stratigraphic framework for the Leichhardt and Calvert superbasins; review and correlations of the pre-1700 Ma successions between Mt Isa and McArthur River. *Australian Journal of Earth Sciences*, *47*(3), 381–403. https://doi.org/10.1046/j.1440-0952.2000.00789.x

Kirilova, M., Toy, V. G., Timms, N., Halfpenny, A., Menzies, C., Craw, D., Beyssac, O., Sutherland, R., Townend, J., Boulton, C., Carpenter, B. M., Cooper, C., Grieve, J., Little, T., Morales, L., Morgan, C., Mori, H., Sauer, K. M., Schleicher, A. M., Williams, J., & Craw, L. (2018). Textural changes of graphitic carbon by tectonic and hydrothermal processes in an active plate boundary fault zone, Alpine Fault, New Zealand. In K. Gessner, T. G. Blenkinsop, & P. Sorjonen-Ward (Eds.), *Characterization of ore-forming systems from geological, geochemical and geophysical studies* (pp. 205–223). Geological Society Special Publications, 453. https://doi.org/10.1144/SP453.13

Kitt, S., Kisters, A., Vennemann, T., & Steven, N. (2018). Orebody geometry, fluid and metal sources of the Omitiomire Cu deposit in the Ekuja Dome of the Damara Belt in Namibia. *Mineralium Deposita*, *53*(2), 261–276. https://doi.org/10.1007/s00126-017-0731-y

Laurent, G., Ailleres, L., Grose, L., Caumon, G., Jessell, M., & Armit, R. (2016). Implicit modeling of folds and overprinting deformation. *Earth and Planetary Science Letters*, *456*, 26–38. https://doi.org/10.1016/j.epsl.2016.09.040

Le, T. X., Dirks, P. H. G. M., Sanislav, I. V., Huizenga, J. M., Cocker, H. A., & Manestar, G. N. (2021a). Geochronological constraints on the geological history and gold mineralization in the Tick Hill region, Mt Isa Inlier. *Precambrian Research*, *366*, 106422. https://doi.org/10.1016/j.precamres.2021.106422

Le, T. X., Dirks, P. H. G. M., Sanislav, I. V., Huizenga, J. M., Cocker, H. A., & Manestar, G. N. (2021b). Geological setting and mineralization characteristics of the Tick Hill Gold Deposit, Mount Isa Inlier, Queensland, Australia. *Ore Geology Reviews*, *137*, 104288. https://doi.org/10.1016/j.oregeorev.2021.104288

Lister, G. S., O'Dea, M. G., & Somaia, I. (1999). A tale of two synclines; rifting, inversion and transpressional popouts at Lake Julius, northwestern Mt Isa terrane, Queensland. *Australian Journal of Earth Sciences*, *46*(2), 233–250. https://doi.org/10.1046/j.1440-0952.1999.00690.x

McKinnon, S. D., & de la Barra, I. G. (1998). Fracture initiation, growth and effect on stress field; a numerical investigation. *Journal of Structural Geology*, *20*(12), 1673–1689. https://doi.org/10.1016/S0191-8141(98)00080-7

Micklethwaite, S., Ford, A., Witt, W., & Sheldon, H. A. (2015). The where and how of faults, fluids and permeability; insights from fault stepovers, scaling properties and gold mineralisation. *Geofluids*, *15*(1-2), 240–251. https://doi.org/10.1111/gfl.12102

Mira Geoscience. (2021). *GOCAD Mining Suite*. Retrieved May 8, 2021, from https://mirageoscience.com/

Mueller, A. G. (2020). Structural setting of Fimiston- and Oroya-style pyrite–telluride–gold lodes, Paringa South Mine, Golden Mile, Kalgoorlie; 1. Shear zone systems, porphyry dykes and deposit-scale alteration zones. *Mineralium Deposita*, *55*(4), 665–695. https://doi.org/10.1007/s00126-017-0747-3

Murphy, T. E. (2004). *Structural and stratigraphic controls on mineralization at the George Fisher Zn-Pb-Ag deposit, northwest Queensland, Australia* [Unpublished PhD thesis]. James Cook University.

Naylor, M. A., Mandl, G., & Supesteijn, C. H. K. (1986). Fault geometries in basement-induced wrench faulting under different initial stress states. *Journal of Structural Geology*, *8*(7), 737–752. https://doi.org/10.1016/0191-8141(86)90022-2

Newberry, S. P., Carswell, J. T., Allnutt, S. L., & Mutton, A. J. (1993). The Dugald River zinc–lead–silver deposit; an example of a tectonised Proterozoic stratabound sulphide deposit. In *World Zinc '93; Proceedings of the International Symposium on Zinc* (pp. 7–21). Australian Institute of Mining and Metallurgy.

O'Dea, M. G., Lister, G., MacCready, T., Betts, P. G., Oliver, N. H. S., Pound, K. S., Huang, W., & Valenta, R. K. (1997). Geodynamic evolution of the Proterozoic Mount Isa terrain. In J-P. Burg & M. Ford (Eds.), *Orogeny through time* (pp. 99–122). Geological Society Special Publications, 121(1). https://doi.org/10.1144/GSL.SP.1997.121.01.05

Page, R. W., & Bell, T. H. (1986). Isotopic and structural responses of granite to successive deformation and metamorphism. *The Journal of Geology*, *94*(3), 365–379. https://doi.org/10.1086/629035

Paradigm. (2021). *SKUA-GOCAD*. Retrieved May 8, 2021, from https://www.pdgm.com/products/skua-gocad

Passchier, C. W., & Trouw, R. A. J. (2005). *Microtectonics* (2nd rev. and enl. ed.). Springer.

Ponce, C., Druguet, E., & Carreras, J. (2013). Development of shear zone-related lozenges in foliated rocks. *Journal of Structural Geology*, *50*, 176–186. https://doi.org/10.1016/j.jsg.2012.04.001

Riedel, W. (1929). Zur mechanik geologischer Brucherscheinungen. *Zentralblatt fur Mineralogie, Geologie und Paleontologie B*, *1929*, 354–368.

Rubenach, M. J., Foster, D. R. W., Evins, P. M., Blake, K. L., & Fanning, C. M. (2008). Age constraints on the tectonothermal evolution of the Selwyn Zone, Eastern Fold Belt, Mount Isa Inlier. *Precambrian Research*, *163*(1-2), 81–107. https://doi.org/10.1016/j.precamres.2007.08.014

Rutter, E. H., Hackston, A. J., Yeatman, E., Brodie, K. H., Mecklenburgh, J., & May, S. E. (2013). Reduction of friction on geologic faults by weak-phase smearing. *Journal of Structural Geology*, *51*, 52–60. https://doi.org/10.1016/j.jsg.2013.03.008

Sanislav, I. V., Dirks, P. H. G. M., Blenkinsop, T., & Kolling, S. L. (2018). The tectonic history of a crustal-scale shear zone in the Tanzania Craton from the Geita Greenstone Belt, NW-Tanzania Craton. *Precambrian Research*, *310*, 1–16. https://doi.org/10.1016/j.precamres.2018.02.025

Scott, D. L., Rawlings, D. J., Page, R. W., Tarlowski, C. Z., Idnurm, M., Jackson, M. J., & Southgate, P. N. (2000). Basement framework and geodynamic evolution of the Palaeoproterozoic superbasins of north-central Australia: An integrated review of geochemical, geochronological and geophysical data. *Australian Journal of Earth Sciences*, *47*(3), 341–380. https://doi.org/10.1046/j.1440-0952.2000.00793.x

Seequent. (2021). *Leapfrog Geo*. Retrieved May 8, 2021, from https://www.seequent.com/

Sibson, R. H. (1990). Conditions for fault-valve behaviour. In R. J. Knipe & E. H. Rutter (Eds.), *Deformation mechanisms, rheology and tectonics* (pp. 15–28). Geological Society Special Publications, 54. https://doi.org/10.1144/GSL.SP.1990.054.01.02

Spampinato, G. P. T., Betts, P. G., Ailleres, L., & Armit, R. J. (2015). Structural architecture of the southern Mount Isa Terrane in Queensland inferred from magnetic and gravity data. *Precambrian Research*, *269*, 261–280. https://doi.org/10.1016/j.precamres.2015.08.017

Spelbrink, L., & George, K-L. (2017). *Dugald River Orebody Knowledge Study (DROKS)*. Unpublished internal MMG report.

Spence, J. S., Sanislav, I. V., & Dirks, P. H. G. M. (2021). 1750–1710 Ma deformation along the eastern margin of the North Australia Craton. *Precambrian Research*, *353*, 106019. https://doi.org/10.1016/j.precamres.2020.106019

Spence, J. S., Sanislav, I. V., & Dirks, P. H. G. M. (2022). Evidence for a 1750–1710 Ma orogenic event, the Wonga Orogeny, in the Mount Isa Inlier, Australia: Implications for the tectonic evolution of the North Australian Craton and Nuna Supercontinent. *Precambrian Research*, *369*, 106510. https://doi.org/10.1016/j.precamres.2021.106510

Stoch, B., Anthonissen, C. J., McCall, M. J., Basson, I. J., Deacon, J., Cloete, E., Botha, J., Britz, J., Strydom, M., Nel, D., & Bester, M. (2018). 3D implicit modeling of the Sishen Mine; new resolution of the geometry and origin of Fe mineralization. *Mineralium Deposita*, *53*(6), 835–853. https://doi.org/10.1007/s00126-017-0784-y

Swanson, M. T. (2005). Geometry and kinematics of adhesive wear in brittle strike-slip fault zones. *Journal of Structural Geology*, *27*(5), 871–887. https://doi.org/10.1016/j.jsg.2004.11.009

Swanson, M. T. (2006). Late Paleozoic strike-slip faults and related vein arrays of Cape Elizabeth, Maine. *Journal of Structural Geology*, *28*(3), 456–473. https://doi.org/10.1016/j.jsg.2005.12.009

Tchalenko, J. S. (1968). The evolution of kink-bands and the development of compression textures in sheared clays. *Tectonophysics*, *6*(2), 159–174. https://doi.org/10.1016/0040-1951(68)90017-6

Tchalenko, J. S. (1970). Similarities between shear zones of different magnitudes. *Geological Society of America Bulletin*, *81*(6), 1625–1639. https://doi.org/10.1130/0016-7606(1970)81[1625:SBSZOD]2.0.CO;2

Tchalenko, J. S., & Ambraseys, N. N. (1970). Structural analysis of the Dasht-e Bayaz (Iran) earthquake fractures. *Geological Society of America Bulletin*, *81*(1), 41–59. https://doi.org/10.1130/0016-7606(1970)81[41:SAOTDB]2.0.CO;2

Vollgger, S. A., Cruden, A. R., Ailleres, L., & Cowan, E. J. (2015). Regional dome evolution and its control on ore-grade distribution; insights from 3D implicit modelling of the Navachab gold deposit, Namibia. *Ore Geology Reviews*, *69*, 268–284. https://doi.org/10.1016/j.oregeorev.2015.02.020

Vollgger, S. A., Wilson, C. J., Micklethwaite, S., Tomkins, A. G., & Cruden, A. R. (2020). Ore shoots in folded and fractured rocks – Insights from 3D modelling of the Fosterville gold deposit (Victoria, Australia). *Ore Geology Reviews*, *118*, 103272. https://doi.org/10.1016/j.oregeorev.2019.103272

Williams, P. F., & Price, G. P. (1990). Origin of kinkbands and shear-band cleavage in shear zones; an experimental study. *Journal of Structural Geology*, *12*(2), 145–164. https://doi.org/10.1016/0191-8141(90)90001-F

Withnall, I. W., & Hutton, L. J. (2013). North Australian Craton. In P. A. Jell (Ed.), *Geology of Queensland* (pp. 23–112). Geological Survey of Queensland.

Xu, G. (1996). Structural geology of the Dugald River Zn–Pb–Ag deposit, Mount Isa Inlier, Australia. *Ore Geology Reviews*, *11*(6), 339–361. https://doi.org/10.1016/S0169-1368(96)00007-8